Physics of Living Systems

Modularity of the segmentation clock and morphogenesis

James E Hammond, Ruth E Baker, Berta Verd

Biology Department, University of Oxford, Oxford, United Kingdom • Mathematical Institute, University of Oxford, Oxford, United Kingdom

https://en.wikipedia.org/wiki/Open_access

Copyright information

A newer version is available. Read the latest version.

Version of Record
April 1, 2025

Reviewed Preprint
v1 • March 11, 2025
Not revised

eLife Assessment

This **valuable** manuscript uses mathematical modeling to address the synchrony of the vertebrate segmentation clock with the developmental processes. The authors use **convincing** arguments to support the idea that this would allow the evolution of flexible body plans and a variable number of segments. This manuscript could be of interest to developmental biologists and systems biologists.

[Editors' note: this paper was reviewed by Review Commons.]

https://doi.org/10.7554/eLife.106316.1.sa4

Abstract

Vertebrates have evolved great diversity in the number of segments dividing the trunk body, however the developmental origin of the evolvability of this trait is poorly understood. The number of segments is thought to be determined in embryogenesis as a product of morphogenesis of the pre-somitic mesoderm (PSM) and the periodicity of a molecular oscillator active within the PSM known as the segmentation clock. Here we explore whether the clock and PSM morphogenesis exhibit developmental modularity, as independent evolution of these two processes may explain the high evolvability of segment number. Using a computational model of the clock and PSM parameterised for zebrafish, we find that the clock is broadly robust to variation in morphogenetic processes such as cell ingression, motility, compaction, and cell division. We show that this robustness is in part determined by the length of the PSM and the strength of phase coupling in the clock. As previous studies report no changes to morphogenesis upon perturbing the clock, we suggest that the clock and morphogenesis of the PSM exhibit developmental modularity.

Introduction

Vertebrates exhibit great diversity in the number of segments that divide the skeleton, musculature, and nervous system of the body, along the rostral-caudal axis (Richardson et al. (1998)). However, the developmental basis for this evolvability remains poorly understood. Segmentation of the body is established by paired blocks of mesodermal tissue, known as somites, that form periodically on either side of the developing embryo as it elongates posteriorly, in a

process known as somitogenesis (Morin-Kensicki et al. (2002); Gomez and Pourquié (2009); Oates et al. (2012)). The total number of segments corresponds to the number of somites formed in the embryo, which is thought to be an emergent property of the morphogenesis of the pre-somitic mesoderm (PSM) and the dynamics of a molecular oscillator known as the segmentation clock (Morin-Kensicki et al. (2002); Cooke and Zeeman (1976); Gomez et al. (2008); Gomez and Pourquié (2009); Harima et al. (2013); Schröter and Oates (2010)). Here, we hypothesise that the evolvability of vertebrate segment number may be underpinned by developmental modularity of the segmentation clock and morphogenesis of the PSM (Raff (1996)), and that the potential of these two processes to evolve independently from one another may explain the diversity observed in vertebrate segment number.

The segmentation clock is a complex gene regulatory network thought to be driven by cell-autonomous oscillations of transcription factors in the Hes/Her family (Palmeirim et al. (1997); Lewis (2003); Harima et al. (2013); Schröter et al. (2012); Webb et al. (2016)). Noisy oscillations are synchronised across cells by delta-notch signalling (Horikawa et al. (2006); Lewis (2003); Venzin and Oates (2020)), creating synchronous travelling waves of gene expression that pulse from the PSM posterior to the anterior. In the anterior PSM somite boundaries are patterned by the interaction of clock oscillations with a posterior-anterior decreasing gradient of FGF signalling that is thought to act as a 'wavefront', reading-out the phase of the clock to create a spatially periodic pattern of somite boundaries (Cooke and Zeeman (1976); Soroldoni et al. (2014); Simsek and Özbudak (2018); Simsek et al. (2023)). The clock synchronises the differentiation of PSM cells as they adopt somite fates at the anterior of the PSM (Cooke and Zeeman (1976)), and so controls both the tempo at which somites are formed, and the anterior-posterior polarity of the somites (Simsek et al. (2023)). Thus, clock synchrony controls the accuracy of somite patterning, and the frequency of clock oscillations determines the frequency of somite formation, which (together with the total duration of somitogenesis), determines the total number of somites formed.

Concurrent with somitogenesis, the PSM undergoes elongation. Comparative studies have shown that a diverse range of mechanisms are responsible for elongation of the PSM (Gomez et al. (2008); Bénazéraf et al. (2010); Steventon et al. (2016); Mongera et al. (2018); Thomson et al. (2021); Michaut et al. (2022)). Importantly, the elongation dynamics of the PSM are thought to control the total duration of somitogenesis which terminates once the PSM becomes sufficiently short in the AP direction (Gomez et al. (2008); Gomez and Pourquié (2009); Steventon et al. (2016)). Therefore, the total number of segments formed in the developing vertebrate is thought to be the product of both the dynamics of the clock (which controls the rate of somite formation), and the morphogenesis of the PSM, via its control on the total duration of somitogenesis.

Developmental modularity is a property of two or more developmental processes where their uncoupling in space or time permits their evolution independently of one another (Raff (1996)). This property is thought to give rise to increased phenotypic diversity by enhancing the evolvability of the system (Raff (1996)). In species examined thus far, such as the Corn Snake *Pantherophis guttatus*, it appears that the evolution of segment number is driven by changes in both the dynamics of the clock and the elongation of the PSM (Gomez et al. (2008)), and it is possible that independent evolution of these two processes is responsible for the high degree of diversity observed in vertebrate segment number. However, it is not obvious whether the two processes are modular, and if so, to what degree. Perturbing the clock's periodicity and function does not appear to affect elongation of the body axis (Schröter and Oates (2010); Forero et al. (2018)), so morphogenesis of the PSM is likely to be robust to changes in the segmentation clock through evolution. However, it is possible that many of the cellular- and tissue-level processes which drive PSM elongation could exert an effect on the dynamics of the clock.

For instance, cell rearrangements thought to drive elongation of the PSM in zebrafish (*Danio rerio*) (Lawton et al. (2013); Mongera et al. (2018)), and in chicken (*Gallus gallus*) (Bénazéraf et al. (2010); Michaut et al. (2022)), promote synchronisation of the segmentation clock (Uriu et al. (2010), 2013); Uriu and Morelli (2014); Uriu et al. (2017)). Additionally arrest of transcription during chromatin condensation is known to cause PSM cells to lag their clock expression relative to neighbours after cell division (Horikawa et al. (2006); Delaune et al. (2012)), causing defects in clock synchrony (Murray et al. (2013)) and suggesting clock synchrony may depend on the degree of proliferative growth in the PSM. The ingression of PSM progenitor cells from dorso-posterior and lateral donor tissues (Kanki and Ho (1997); Steventon et al. (2016); Xiong et al. (2020)) can also create clock asynchrony, as incoming progenitor cells do not appear to show clock gene expression (Mara et al. (2007)) and thus may be asynchronous with their neighbours when they enter the PSM. Finally, tissue convergence movements associated with the elongation of the PSM (Thomson et al. (2021)) have been proposed to negate the effect of random cell mixing and be deleterious for clock synchronisation (Uriu and Morelli (2014)). It is thus non-trivial to determine whether the duration and rate of somitogenesis are modular since, in order to do so, one must examine the effect of varying morphogenesis on the dynamics of the clock.

To do this, we use a computational approach to simulate clock dynamics and cell movements within the PSM, and study how the clock responds to changes in morphogenesis. We use this approach as it is much quicker and more flexible than experimentally manipulating morphogenesis *in vivo*. As we are constrained by computational complexity and cannot simulate all possible means by which the PSM can elongate (this would require simulation of the growth and dynamics of cells in surrounding tissues which exert forces on the PSM (Xiong et al. (2020))), we limit our study to simulating regimes of cell movement and growth within the PSM that are known to be associated with, or causal in, PSM growth and elongation across vertebrates.

We use a previously established three-dimensional model of cell movements and clock dynamics within the zebrafish PSM (see **figure 1A**) (Uriu et al. (2021)), and adapt this model to simulate various regimes of cell movement and growth. Briefly (a more detailed description of the model can be found in the methods), the model assumes the PSM is in an inertial frame of reference, with elongation being encoded by the advection of cells towards the anterior PSM (the anterior limit of which is denoted $x = x_a$, see **figure 1A**). Besides advection, cells are subject to random cell mixing, cell-cell repulsion, and a boundary force confining the cells within a hollow horseshoe-shaped domain. This model uses a phase-oscillator approach to describe segmentation clock dynamics and each cell is assigned a clock phase which is frozen when the cell exits the PSM at $x = x_a$, crossing the wavefront and patterning a segment (**figure 1A**). To replenish cells lost at the anterior, new cells are added with random phase and position to keep the tissue at a constant density (**figure 1B**).

This model is appealing for several reasons, the first being that the model is three-dimensional and so can quantitatively recapture the rates of cell mixing that we observe within the PSM (Uriu et al. (2017), 2021). The second is that the segmentation clock is described by an abstract phase-oscillator, broadly agnostic to the molecular details which are known to vary between vertebrates (Krol et al. (2011)). Finally, the model makes extensive use of experimentally-derived parameters for cell movements, tissue dimension, and the phase-oscillator model of the clock in zebrafish (Uriu et al. (2021)). This allows us to make quantitative predictions as to how the zebrafish segmentation clock would react to changes in PSM morphogenesis.

Using this model we test the clock's response to changes in the position of cell ingression into the PSM, changes in the anterior-posterior profile of random cell motility, changes in the length and density of the PSM, and to mitosis. We find that the clock's synchrony and frequency are robust to these changes except when mitosis is introduced, where we find that synchrony is negatively impacted except where mitosis is confined to the posterior PSM. We find that this robustness is

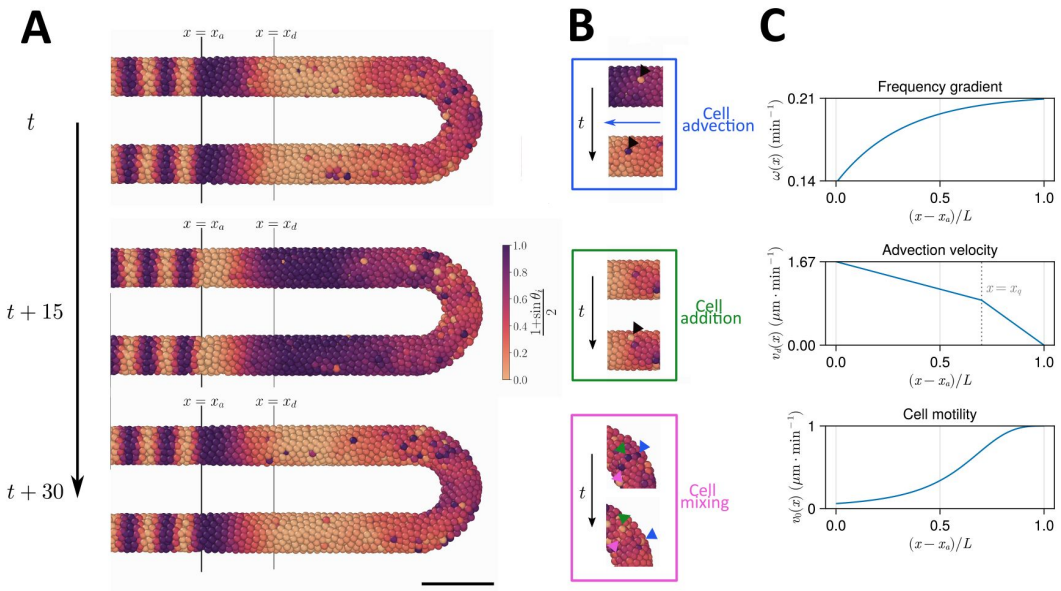

Figure 1.

Computational model of the clock and the PSM.

A Stills of a simulation of the model of Uriu et al. (2021). Kinematic phase (θ_i) waves emerge in the posterior (right) and travel towards the tissue anterior (left, $x = x_a$), where phase is arrested. The model is parameterised to data from zebrafish, and accordingly the clock oscillates every 30 minutes. **B** Insets illustrating the key processes driving cell movements in the PSM within the model. Top: Cells advect towards the anterior of the tissue, simulating elongation of the PSM. Middle: New cells are added to replenish the loss of cellular material as cells advect towards the anterior. Bottom: Cells undergo motility-driven rearrangements. **C** Functions in the model describing (top) the intrinsic oscillation frequency, (middle) the advection velocity, (bottom) and the motility, of each cell depending on its normalised position along the anterior-posterior axis, ($x - x_a/L$). Plots were generated using the parameters given by Uriu et al. (2021).

underpinned by the tissue length and cell density in the model, as well as the rate of cell mixing and strength of clock phase coupling. Together, these results suggest that segmentation clock dynamics and PSM morphogenesis are modular components of somitogenesis that can evolve independently from one another, conferring evolvability and helping to explain the diversity in segment number across the vertebrates.

Results

Varying the position of cell ingression has minimal effect on clock dynamics

During somitogenesis new cells enter the PSM posteriorly via ingression from dorsal tissues (Kanki and Ho (1997); Banavar et al. (2021)). In the early stages of zebrafish somitogenesis, there is also a contribution of cells from lateral tissues (Steventon et al. (2016)). As ingressing cells do not appear to express segmentation clock genes (Mara et al. (2007)), the position at which cells ingress into the PSM can create challenges for clock patterning, as only in the 'off' phase of the clock will ingressing cells be synchronous with their neighbours. Therefore continuous ingression of PSM progenitor cells is likely to create local asynchrony of oscillations where it occurs, and so varying the position of cell ingression may have an effect on clock dynamics at the wavefront.

To test this hypothesis, we alter how cells are added to the tissue in the model. To model the ingression of cells from dorsal tissues into the posterior tailbud (Kanki and Ho (1997); Banavar et al. (2021)), we define a density-dependent cell addition process where cells are added onto the dorsal surface of the posterior half-toroid domain (see **figures 2A 8**) if the average density in this domain falls below ρ_0, with a constant initial phase $\theta = 0$. To maintain equal density across the PSM, we found it necessary to add cells in the two cylindrical PSM domains as well, as when cells were only added to the posterior half-toroid domain we observed a loss in density in the two cylindrical domains (data not shown). To avoid bias we add cells at random positions if the average density falls below ρ_0. These cells are initialised with a random phase drawn from the uniform distribution $[0, 2\pi)$. To model the early stages of zebrafish somitogenesis where, concurrent with dorso-posterior ingression of cells, the PSM also experiences a contribution of cells from lateral tissues, we modify the above simulation so that cell density in the lateral cylindrical domains is maintained by addition of cells with constant phase ($\theta = 0$) on the ventral surface of these two lateral domains (see **figures 2A** 8). These two ingression scenarios are termed 'Dorso-Posterior' ('DP') and 'Dorso-Posterior + Lateral-Ventral' ('DP+LV') ingression (**figure 2A**), respectively, and for brevity we refer to them as 'DP' and 'DP+LV' in the rest of the text. We compare the effect of these scenarios of cell ingression with 'Random' ingression (**figure 2A**), where cell density is maintained by addition of cells at random positions within the tissue with random phase ($\theta \in [0, 2\pi)$).

We test these scenarios by initialising each simulation with a synchronous initial condition for the clock and simulating cell movements and clock dynamics in the presence of each cell ingression scenario for 1000 mins (see methods for further justification). After 1000 mins we measure the synchrony (r) and mean frequency ($\mathrm{d}\theta/\mathrm{d}t$) of a cylindrical region of tissue at the left-hand PSM anterior, one cell diameter (d_c) in length (see methods). We restrict our measurement to the PSM anterior as it is here that the clock patterns somites (Simsek and Özbudak (2018); Simsek et al. (2023)), and thus dynamics elsewhere in the tissue are unlikely to present a phenotype in the animal. Using this method, we find that DP ingression has no effect on synchrony at the PSM anterior after 1000 mins when compared to Random ingression, but that DP+LV ingression creates a minor decrease in anterior synchrony (**figure 2B**). However, in neither scenario is the anterior frequency changed when compared to Random ingression (**figure 2C**). Kymographs of synchrony along the anterior-posterior axis reveal that cell addition onto the tissue surface creates

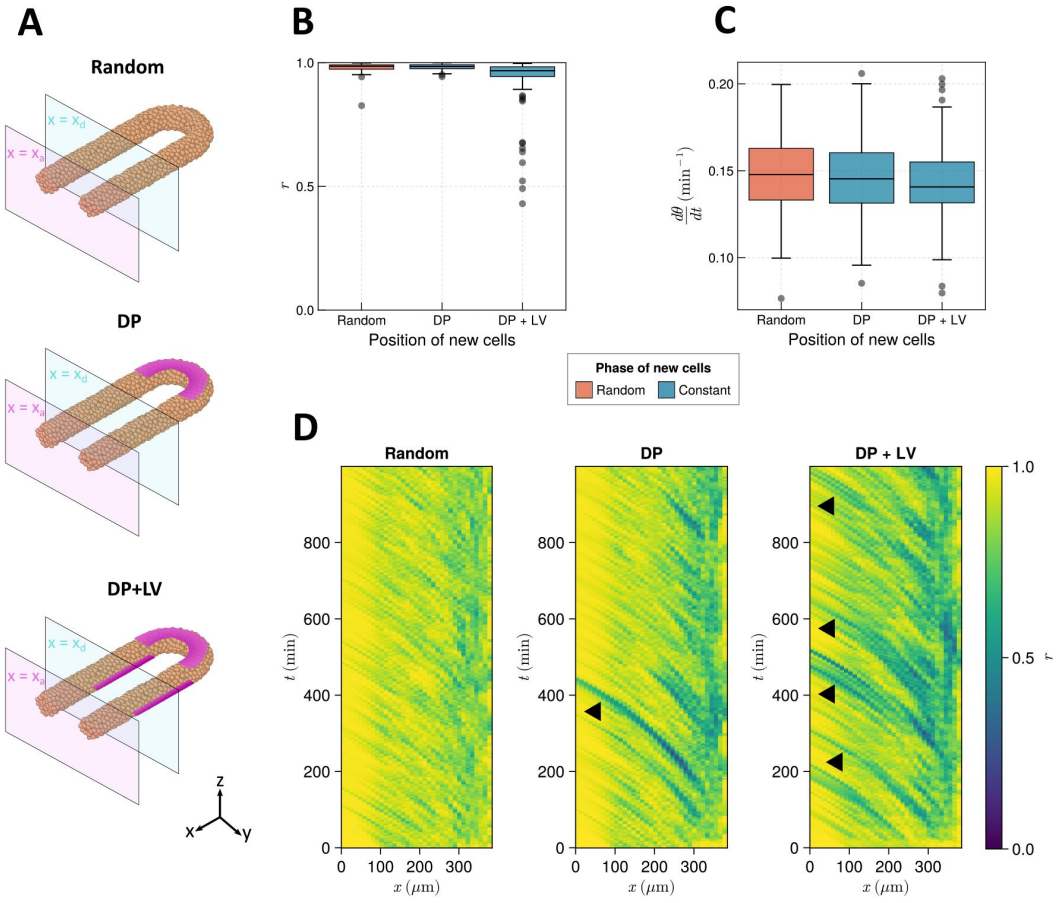

Figure 2.

The effect of cell ingression position on clock frequency and synchrony.

A Diagram highlighting the position of cell addition across the three ingression scenarios tested here. Magenta shading shows where cells are added onto the tissue surface. The pale magenta and blue planes respectively correspond to the anterior limit of the PSM, $x = x_a$, and the anterior limit of cell addition, $x = x_d$. In the 'Random' condition cells are added at random positions within the PSM posterior to the plane $x = x_d$, and accordingly no magenta surface is shown. Similarly in the dorso-posterior case ('DP') cells are added at random positions in the two lateral cylinders to maintain density, and no magenta surface is shown there. In the dorso-posterior + lateral-ventral ('DP+LV') case cells are only added on the tissue surface at the positions shown by magneta shading. **B** Oscillation synchrony (r) at the PSM anterior after 1000 mins, for the three tested scenarios of cell ingression. N=100 simulations. **C** Mean frequency of oscillations for cells at the PSM anterior after 1000 mins of simulation, for the three tested scenarios of cell ingression. N=100 simulations. **D** Kymographs of synchrony along the x-axis on the left-hand side of the PSM for single simulations from each of the three scenarios of cell ingression tested. Black arrowheads highlight strongly asynchronous populations of cells being transported to the tissue anterior by advection.

asynchronous populations of cells that travel towards the tissue anterior with cell advection (**figure 2D**, black arrowheads). These are more frequent than in the DP case, likely explaining the lower anterior synchrony observed in the DP+LV simulations.

The clock is robust to changes in mode of cell ingression regardless of the cell motility profile

As cell mixing promotes clock synchrony (Uriu et al. (2010, 2013); Uriu and Morelli (2014)), and an anterior-posterior profile of increasing cell mixing is present in the PSM of zebrafish and chicken (Kanki and Ho (1997); Bénazéraf et al. (2010); Lawton et al. (2013); Mongera et al. (2018); Michaut et al. (2022)) (and presumably most vertebrate taxa), we speculated that the shape of this gradient may confer robustness to clock dynamics against cell ingression. For instance, a steep profile (e.g. as reported from the early somitogenesis stages of zebrafish (Mongera et al. (2018))) might confer robustness to lateral ingression as mixing is higher along a greater length of the PSM than a more graded profile (e.g. as reported from chicken embryos (Bénazéraf et al. (2010); Michaut et al. (2022))). Therefore the shape of the cell motility profile in the PSM may constrain the evolution of cell ingression position, and vice versa.

To test this, we systematically enumerated the steepness (h) and inflexion point (X_v) of the function $v_0(x)$ (**figure 3B**), which controls the speed of random cell movement in the PSM (see methods, **figure 3A**). For each parameter pair we performed $N = 100$ simulations and recorded the median anterior synchrony and median anterior mean frequency ($\mathrm{d}\theta/\mathrm{d}t$, see methods) after 1000 mins. The results for each ingression scenario are shown in **figure 3C**. We find no trend in median anterior synchrony and frequency across different parameter pairs for Random ingression, DP ingression, or DP+LV ingression (**figure 3C**). Similar to before, results for DP ingression are indistinguishable from Random ingression. For DP+LV ingression, anterior synchrony is lower across all parameter sets than DP ingression or Random ingression (**figure 3C**) but the effect is still very minor in this case. We therefore predict that, at least with respect to effects on the zebrafish segmentation clock, the evolution of the motility profile and the position of cell ingression are not constrained by one another.

Length and density of the PSM confer robustness to the clock

The PSM is a transient tissue that shrinks in length over time. While this feature is conserved across vertebrate species, the absolute length and rate of shrinkage are known to vary between taxa (Gomez et al. (2008); Steventon et al. (2016); Thomson et al. (2021)). We postulate that PSM length is an important factor in determining the clock's response to different morphogenetic modes; for example, intuitively cells will have more time to synchronise oscillations with their neighbours before reaching the PSM anterior in a longer PSM, or if cell ingression is spread out along a longer tissue the degree of asynchrony imparted by ingression will be lessened. Similarly, we predict that the density of the tissue confers robustness to clock dynamics as increasing the average number of neighbours for each cell may act to 'correct' against clock noise. Overall, tissue density has been observed to increase over time in zebrafish (Thomson et al. (2021)), and has been observed to vary in space in chicken, with density decreasing towards the PSM posterior (Bénazéraf et al. (2010); Michaut et al. (2022)).

We thus sought to explore whether the length and density of the PSM confer robustness to changing morphogenesis. We test this by co-varying the position of cell ingression (**figure 2A**) with either tissue density or length. When varying the average tissue density ρ_0 and studying model dynamics after 1000 mins we see that increasing cell density marginally increases anterior synchrony (**figure 4B**), and decreases the variability in frequency at the PSM anterior (**figure 4C**). However the increase in density does not appear to be sufficient to 'correct' the decrease in synchrony in the DP+LV case (**figure 4B**). Increasing the length of the tissue does however appear to 'correct' this decrease (**figure 4E**). Here the PSM length L is increased but the anterior

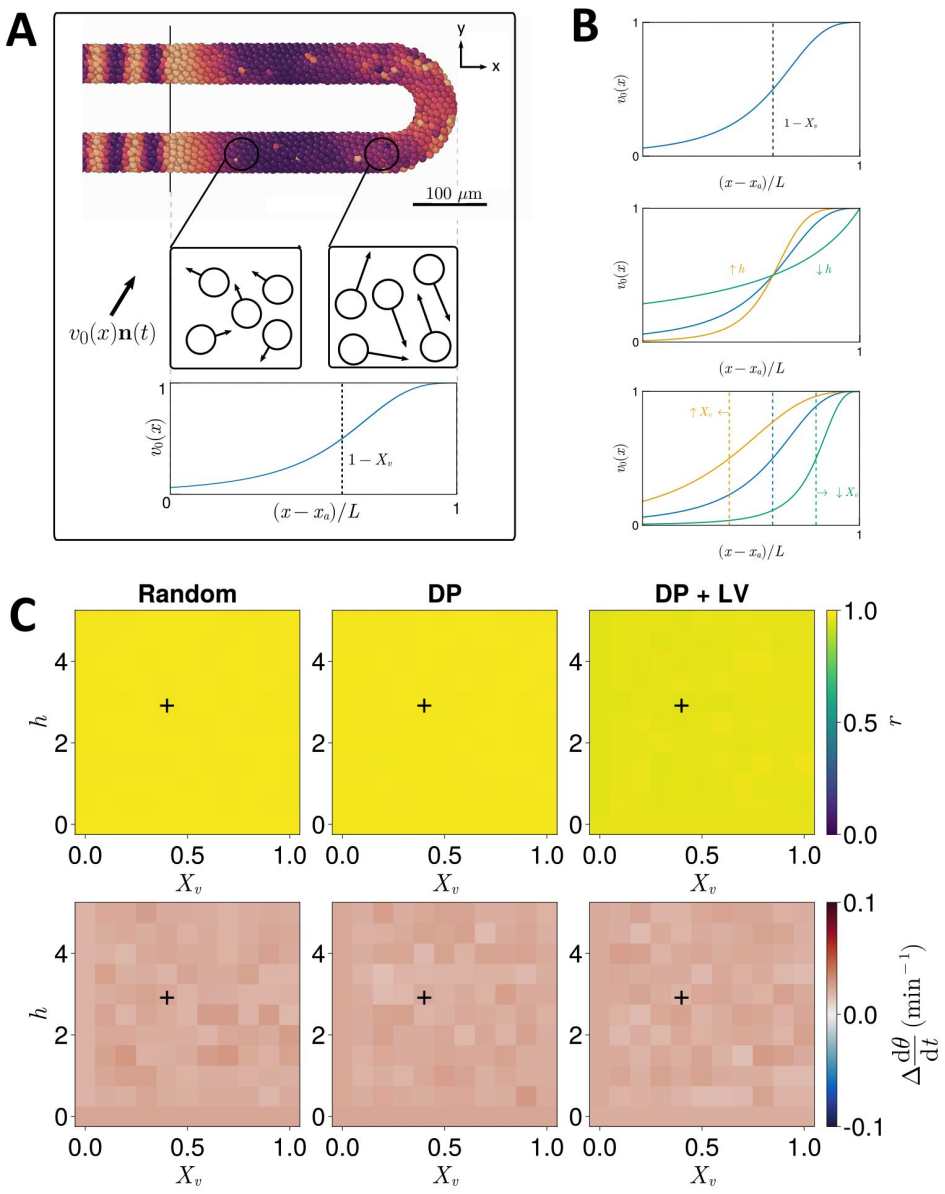

Figure 3.

Effect of cell motility profile on clock frequency and synchrony.

A Overview of how intrinsic cell motion is encoded in the model. Each cell is given a random direction vector $v_0(\mathbf{x}_i)\mathbf{n}_i(t)$ (black arrows) whose magnitude $v_0(\mathbf{x}_i)$ increases towards the PSM posterior. **B** Magnitude of intrinsic cell motion $v_0(\mathbf{x})$ for the parameters used by Uriu et al. (2021) (blue), and how the shape of the function can change when increasing (yellow) or decreasing (green) the inflexion point and curve steepness parameters, X_v and h, respectively. **C** Clock synchrony r (**top**) and difference from expected mean frequency $\Delta d\theta/dt$ (**bottom**) for different $v_0(\mathbf{x})$ specified by combinations of X_v and h. The corresponding pixels display the synchrony or frequency at the PSM anterior after 1000 mins of simulation using the specified motility profile, averaged across $N = 100$ simulations. Parameter ranges used are $X_v \in \{0, 0.1, 0.2, ..., 1\}$ and $h \in \{0, 0.5, 1, ..., 5\}$.

limit of cell addition x_d is held constant at x_d = 100 μm. Anterior synchrony after 1000 mins positively correlates with L, and decreasing L reveals a decrease in anterior synchrony for DP ingression (**figure 4E**). No obvious trend for mean anterior frequency is observed (**figure 4F**). Note that the results for the DP and DP+LV cases are exactly equal for L = 185 μm, as for x_d = 100 μm cell addition is confined to the dorsal-posterior domain and the two ingression methods are numerically equivalent in the model (see methods). While much of this recovery in synchrony may be due to cell addition occurring along a longer domain (and in so doing 'diluting' the effect of cell ingression), we observe similar results when cell addition can only occur along a fixed length of the tissue and the total length of the tissue varies (**figure 4** supplementary figure 1). Here, the anterior limit of cell addition x_d is fixed in relation to the length of the PSM, by $x_d = L - R - r - 100$ (where R represents the major radius of the half-toroid domain and r the radius of the PSM tube, see **figure 8**), and we observe a recovery in synchrony across all three cell ingression scenarios as the total length of the tissue increases (**figure 4** supplementary figure 1).

However in zebrafish density and length are known to co-vary after the 16-somite stage (ss), with the PSM increasing in density as it shrinks in length (Thomson et al. (2021)). We would expect decreasing the length of the PSM to decrease the clock's robustness to noise, but it is possible that the concurrent increase in density is sufficient to counteract this and preserve clock dynamics. As the dynamics of somitogenesis are consistent across individuals at these late stages (Schröter et al. (2008)), the dynamics of the zebrafish segmentation clock are likely unaffected by compaction-extension of the PSM. It is not clear however if this can be explained by the concurrent changes in PSM length and density that occur during compaction-extension or if clock properties such as phase-coupling need to vary in order to maintain robust clock dynamics.

Here we simulate compaction-extension by shrinking the PSM radius r and length L, while increasing its density ρ, over time, using published rates and initial conditions for these values (**figure 5A-B**, methods) (Thomson et al. (2021)). We also decrease the cell diameter d_c, as has been observed in zebrafish (Thomson et al. (2021)), as we expect this to be important in determining clock dynamics by changing the number of neighbouring cells that a given cell can couple its phase to.

As these changes are dynamic, we depart from previous methodology for measuring clock dynamics and plot the anterior synchrony and frequency over time for N=100 simulations. For small PSM lengths and widths the model generates voids in the tissue as cells do not exit the toroid domain at a sufficient rate to maintain tissue homogeneity, which we deem to be biologically inaccurate. To exclude such cases we only plot synchrony and frequency up until the time at which one of the N=100 replicate simulations encounters such a gap. Thus it is important to note that the simulations presented here do not cover the whole timespan of zebrafish somitogenesis, and we cannot examine dynamics towards the end of the process.

The anterior synchrony and mean anterior frequency over time for N = 100 simulations of compaction-extension are shown in **figures 5C** and **5D**, respectively. They are compared with simulations that do not shrink the PSM and maintain constant L, r, d_c, and ρ. We find that towards the end of these simulations the clock experiences more noise and fluctuations in synchrony and frequency (**figure 5C-D**) than the non-shrinking equivalent simulations, however for the majority of the simulation the dynamics of the compacting tissue are broadly comparable with those of the non-compacting tissue, but with synchrony minorly decreasing and frequency becoming noisier towards the end of the simulation (**figure 5C-D**). We treat the effects observed towards the end of the simulation with caution in light of the irregularities in tissue structure mentioned above. In addition, other model parameters that are fixed throughout the simulation, such as advection velocity or intrinsic frequency, are thought to change towards the end of somitogenesis (Schröter et al. (2008); Uriu et al. (2021)), and therefore for the latter stages of somito-genesis the results of our simulations may be inaccurate. However, data for the final stages of zebrafish somitogenesis is extremely limited and we cannot make estimates for model

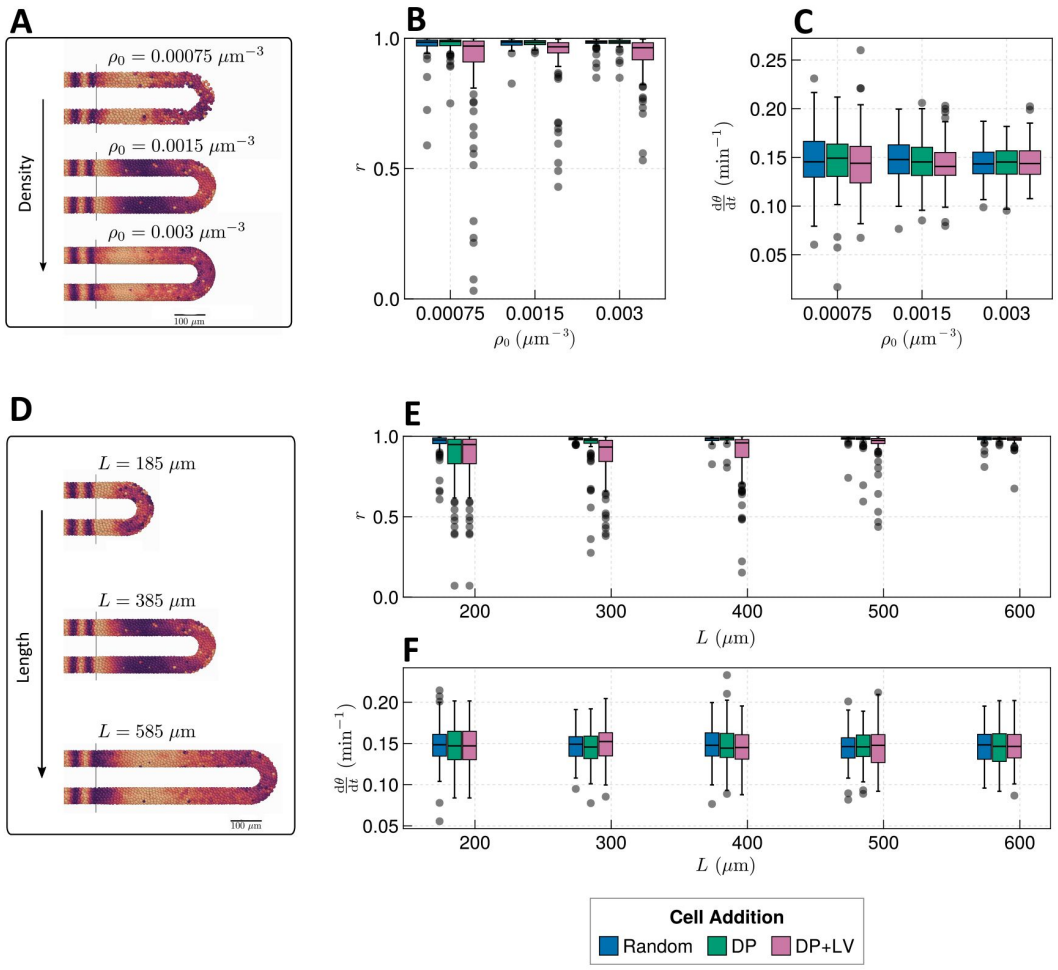

Figure 4.

Effect of tissue density and length.

A Stills from exemplar simulations illustrating the impact of changes in tissue density ρ_0. **B** Anterior synchrony after 1000 mins for changing tissue density ρ_0 and varying position of cell ingression. N=100 simulations. **C** Anterior mean frequency after 1000 mins for changing tissue density ρ_0 and varying position of cell ingression. N=100 simulations. **D** Stills from exemplar simulations illustrating changes in tissue length. **E** Anterior synchrony after 1000 mins for changing tissue length L and varying position of cell ingression. N=100 simulations. **F** Anterior mean frequency after 1000 mins for changing tissue length L and varying position of cell ingression. N=100 simulations.

Figure 4—figure supplement 1.

Effect of co-varying coupling strength κ, tissue length L, and position of cell ingression on the median anterior synchrony of N=100 simulations. A black + corresponds to the parameter pair used elsewhere in this paper, unless otherwise stated (L = 385 μm, κ = 0.07 min^{-1}).

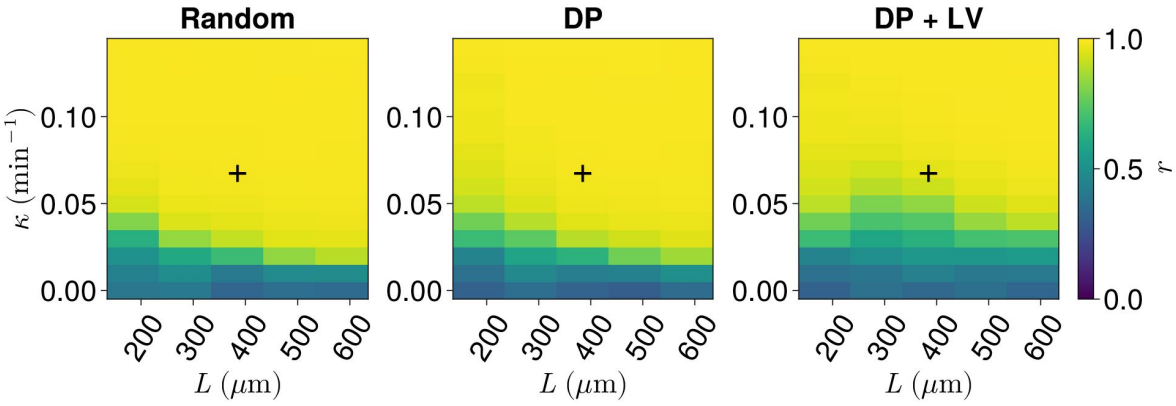

Figure 4—figure supplement 2.

Top Anterior synchrony after 1000 mins for changing tissue length L and varying position of cell ingression, where x_d is fixed at $x_d = L - R - r - 100$. N=100 simulations. **Bottom** Anterior mean frequency after 1000 mins for changing tissue length L and varying position of cell ingression where $x_[d]$ is fixed at $x_d = L - R - r - 100$. N=100 simulations.

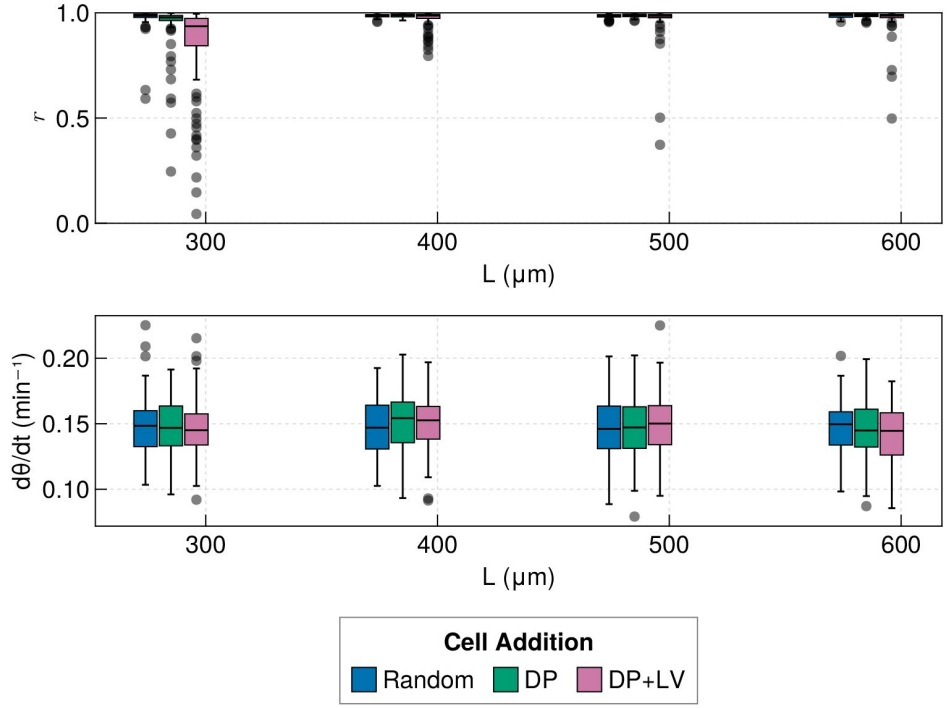

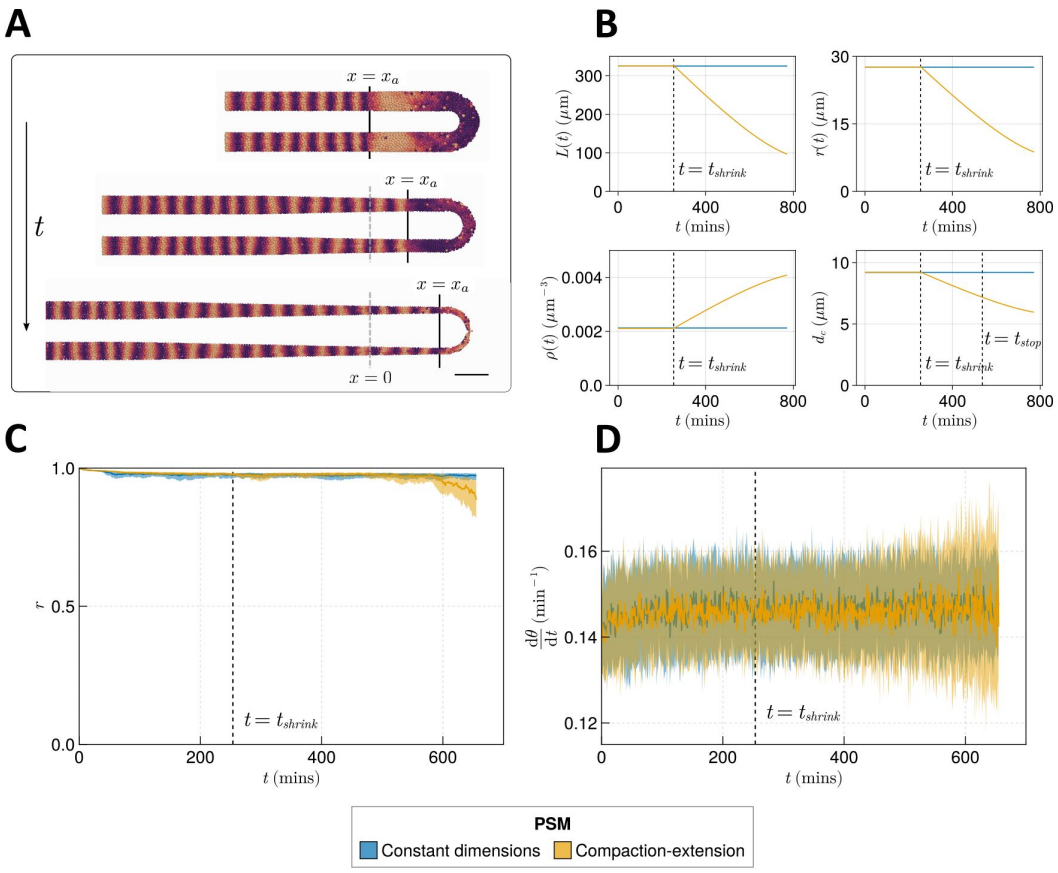

Figure 5.

Effect of compaction-extension on clock synchrony and frequency.

A Snapshots of an exemplar simulation showing how the PSM shrinks in length and diameter as time progresses. **B** Functions for PSM length *L*, radius *r*, density *ρ*, and cell diameter d_c, derived from (Thomson et al. (2021)) (yellow), and the constant functions (blue) with which the effect of these functions is compared. **C** Anterior synchrony and **D** mean anterior frequency over time, for N=100 simulations. The solid line indicates the median and the inter-quartile range is given by a shaded band either side of this line. Blue shows simulations where the tissue does not undergo compaction-extension after t_{shrink}, and yellow shows the results for simulations where after t_{shrink} the tissue undergoes compaction-extension according to the functions shown in **B**. Results are plotted until the time at which at least one of the replicate simulations encounters a gap in the tissue at the tissue anterior (see methods).

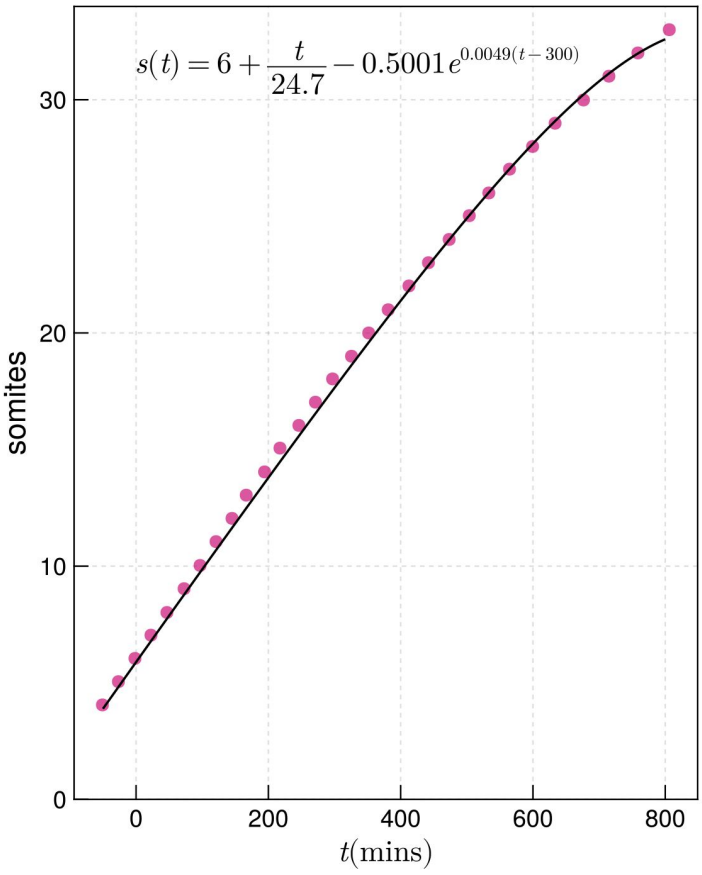

Figure 5—figure supplement 1.

Fitted function interpolating the data for zebrafish somitogenesis from Schröter et al. (2008) (black), against the raw data (magenta).

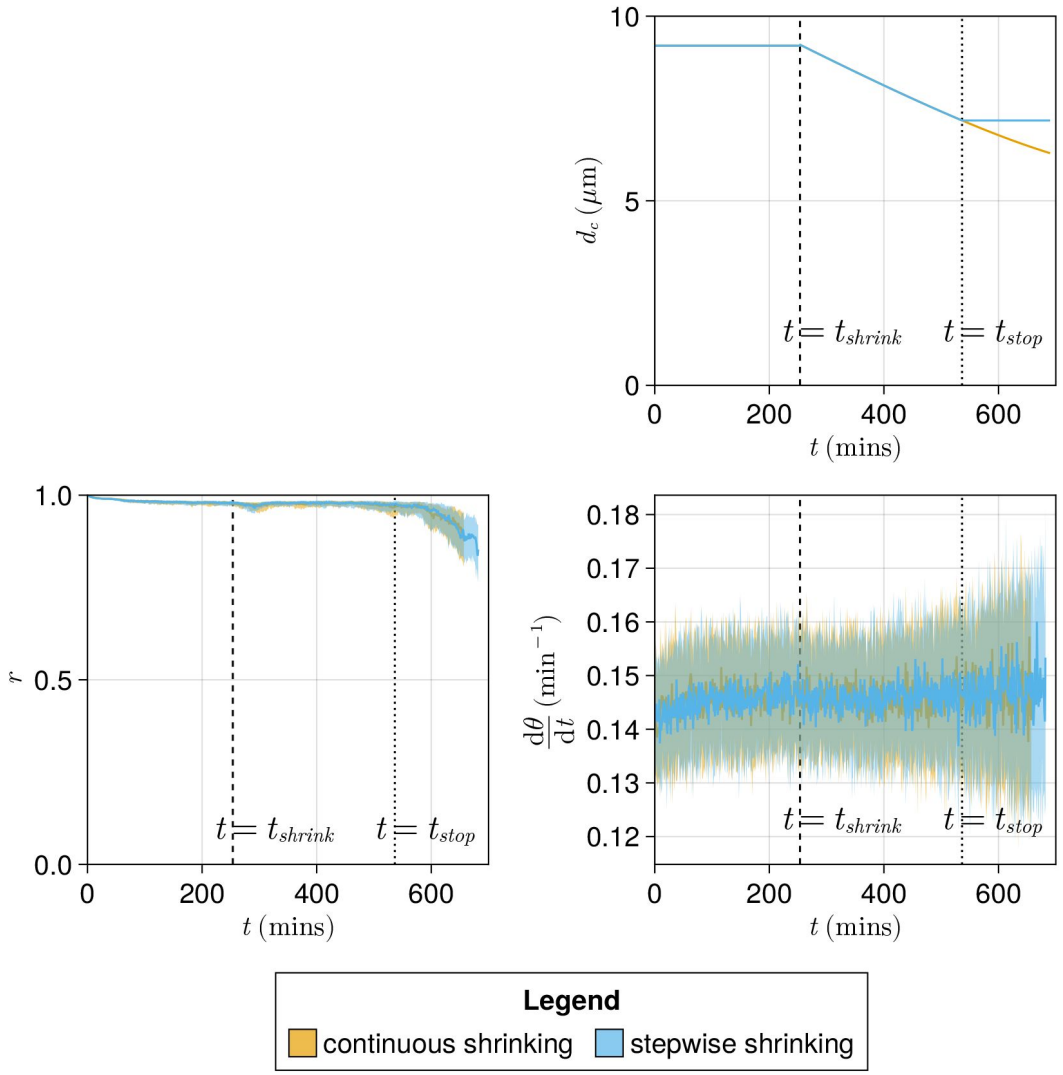

Figure 5—figure supplement 2.

Comparing the choice of a 'stepwise' function for decreasing cell diameter d_c against a function where d_c decreases continuously until the simulation's end. **A** The stepwise (blue) and continuous (yellow) functions compared here. The intercept and gradient for these functions are derived from data from Thomson et al. (2021). **B** Anterior synchrony (r) over time for stepwise shrinking cells (blue) and continuously shrinking cells (yellow). Dark line shows the median of N=100 simulations, and the shaded area either side of this line shows the inter-quartile range (IQR). Results are plotted until the time at which at least one of the replicate simulations encounters a gap in the tissue at the tissue anterior (see methods). **C** Mean anterior frequency ($d\theta/dt$) over time for stepwise shrinking cells (blue) and continuously shrinking cells (yellow). Dark line shows the median of N=100 simulations, and the shaded area either side of this line shows the IQR. Results are plotted until the time at which at least one of the replicate simulations encounters a gap in the tissue at the tissue anterior.

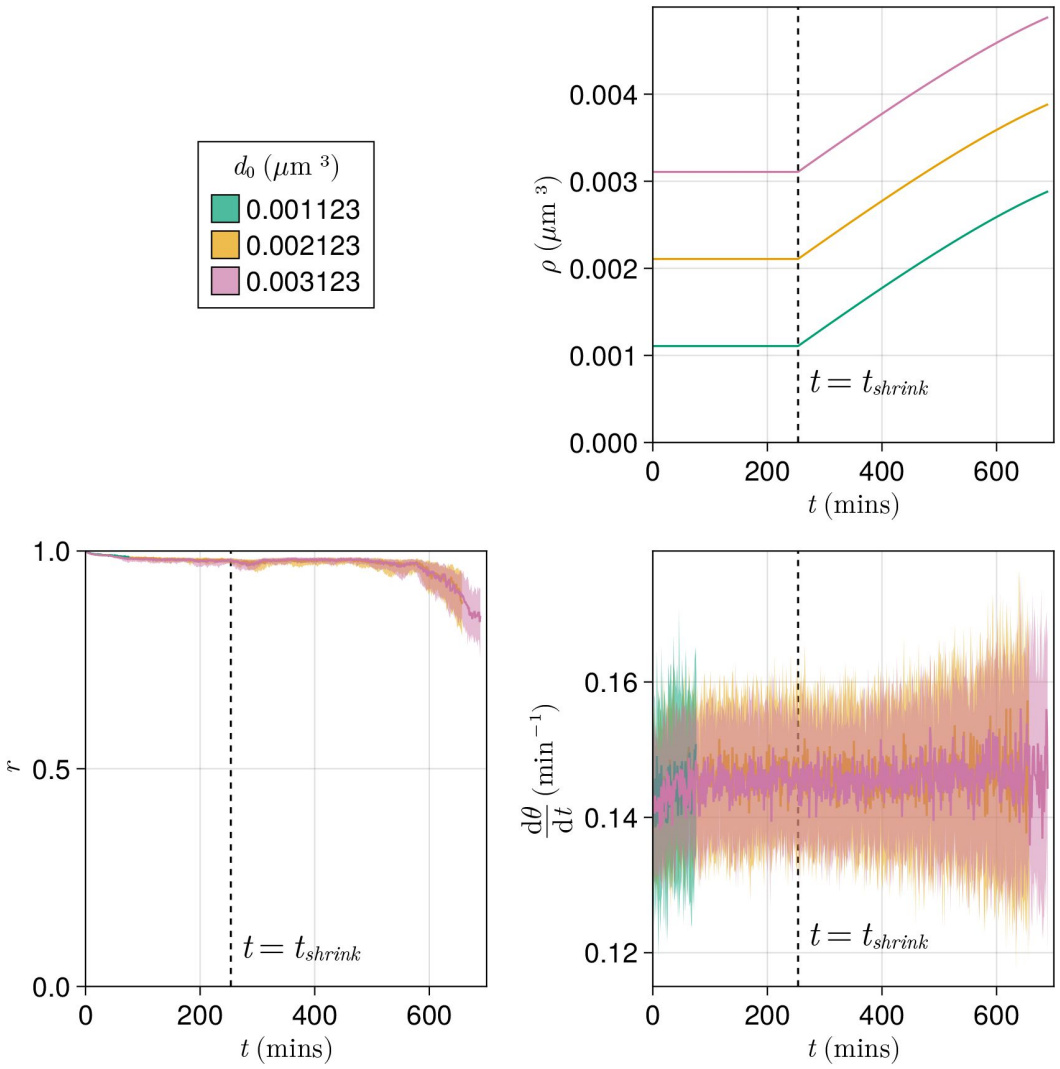

Figure 5—figure supplement 3.

Effect of starting tissue density d_0 on anterior synchrony and frequency over time, for a compacting tissue. **A** Functions showing tissue density $\rho(t)$ for different intercept values d_0. **B** Anterior synchrony (r) over time. Dark line shows the median of N=100 simulations, and the shaded area either side of this line shows the inter-quartile range (IQR). Results are plotted until the time at which at least one of the replicate simulations encounters a gap in the tissue at the tissue anterior (see methods). **C** Mean anterior frequency ($d\theta/dt$) over time. Dark line shows the median of N=100 simulations, and the shaded area either side of this line shows the IQR. Results are plotted until the time at which at least one of the replicate simulations encounters a gap in the tissue at the tissue anterior.

parameters at this stage. Therefore we conclude that for much of somitogenesis in zebrafish the clock is not majorly impacted by the compaction-extension of the tissue, but that there may be effects at the terminal stages of somitogenesis undetected by this model.

Beyond dynamic changes in density, we also attempted to encode a spatial gradient of decreasing cell density towards the posterior, as reported from chicken (Bénazéraf et al. (2010); Michaut et al. (2022)). However, we could not generate a gradient that quantitatively recaptures that reported by Bénazéraf et al. (2010) (data not shown). Based on our results for changing average cell density ρ_0 (**figure 4B-C**) it is highly probable that this gradient would affect clock dynamics. We suggest that another model, such as one encoding cell-cell adhesion, may be a more powerful tool for exploring the effect of this gradient, and dynamics at the terminal stages of somitogenesis.

Clock arrest during cell division creates asynchrony

During M phase of the cell cycle, segmentation clock gene expression in zebrafish is known to arrest (Horikawa et al. (2006)), causing a lag in nascent daughter cells relative to their neighbours (Delaune et al. (2012)). If cell divisions are asynchronous, as appears to be the case in zebrafish (Kanki and Ho (1997); Steventon et al. (2016)), then such lags can create asynchrony of oscillations in the tissue (Murray et al. (2013)).

As previous models of mitosis and the segmentation clock have been two-dimensional and therefore may not quantitatively recapture the cell mixing and geometry present in zebrafish (Murray et al. (2013), 2019), we sought to investigate the effect of mitosis in the presence of the more accurate three-dimensional geometry and cell mixing. To do so, we simulated cell division by assigning each cell a cell cycle phase τ that increases at a constant rate of 1 min^{-1}, and spawning a new cell adjacent to that cell once that its $\tau \geq T_G + T_M$, where T_G denotes the total time in minutes to complete G1, S, and G2 phases of the cell cycle, and T_M denotes the time spent in M phase, in minutes. Once a daughter cell is generated, the τ for both cells is reset to zero. As daughter cells share the same clock phase after division *in vivo* (Delaune et al. (2012)), the daughter cell shares the same clock phase θ as its sibling. To simulate the arrest of the clock during M phase, if $\tau \in [T_G, T_G + T_M)$ oscillations cease, i.e. $\mathrm{d}\theta_i/\mathrm{d}t = 0$. For further details, we refer the reader to the methods section below.

To avoid measuring trivial changes in frequency and synchrony due to arrest of the clock, we measure synchrony and frequency of the clock only in cells where $\tau < T_G$. Therefore our results represent a lower bound on the effect of mitosis on the clock. Using the estimated values of T_G and T_M for zebrafish (see methods for calculation), we find that the presence of cell division creates asynchrony as reported previously (Murray et al. (2013)), and has no identifiable effect on frequency (**figure 6B-C**). Fixing $T_G + T_M = 187.5$ mins and varying T_M shows a T_M-dependent trend where synchrony decreases with increasing T_M (**figure 6E**). After $T_M = 15$ mins the synchrony recovers slightly but remains noisy (**figure 6E**). No noticeable trend is observed for the frequency (**figure 6** supp 1A).

In previous simulations (**figure 6**), cell division occurs up to the wavefront where segments are pre-patterned ($x = x_a$). However if division is confined to the posterior (Bouldin et al. (2014)) cells may have time to re-synchronise before reaching the wavefront. To test whether this is possible within the timescales of zebrafish cell movement, division, and clock dynamics, we define a point in space $x = x_a + x_{div}$ anterior to which (i.e. for $x < x_a + x_{div}$) we halt cell cycle progression by fixing $\tau = 0$ mins in all cells. Performing simulations with $x_{div} = 25\mu\text{m}$, $175\mu\text{m}$, $325\mu\text{m}$, we see that while for $x_{div} = 25\mu\text{m}$ we observe defects in synchrony, for $x_{div} = 175\mu\text{m}$, $x_{div} = 325\mu\text{m}$, synchrony is rescued (**figure 6D**). This suggests that there exists some point along the PSM's AP axis posterior to which cell division can occur without affecting the anterior dynamics of the clock. To try and resolve the value of this point and how it depends on the length of M-phase T_M, we systematically enumerated values of x_{div} from the tissue anterior to the tissue posterior, and T_M across the values tested in **figure 6E**. We find that for $T_M < 15$ mins division can occur up to the

Figure 6.

Effect of cell division on clock frequency and synchrony.

A Diagram showing how during cell division, clock phase θ arrests, causing a cell to fall out of phase with its neighbour. On the right hand side a still from a simulation for T_M = 15 mins is shown, illustrating how this creates asynchrony of oscillations. The effect of cell division on anterior synchrony and frequency is shown in figures **B** and **C**, respectively, for T_M = 15 mins after 1000 mins. N = 100. **D** The effect on anterior synchrony when division is restricted to only occur posterior to $x = x_{div}$, for T_M = 15 mins. N = 100. **E** The effect on anterior synchrony after 1000 mins when T_M is varied. In each case, the total length of the cell cycle is maintained at a constant length, i.e. $T_M + T_G$ = 187.5 mins. N = 100. To rule out trivial changes in synchrony and frequency, in all analysis here we restrict measurement to non-dividing cells, i.e. cells such that $\tau \in [0, T_G)$.

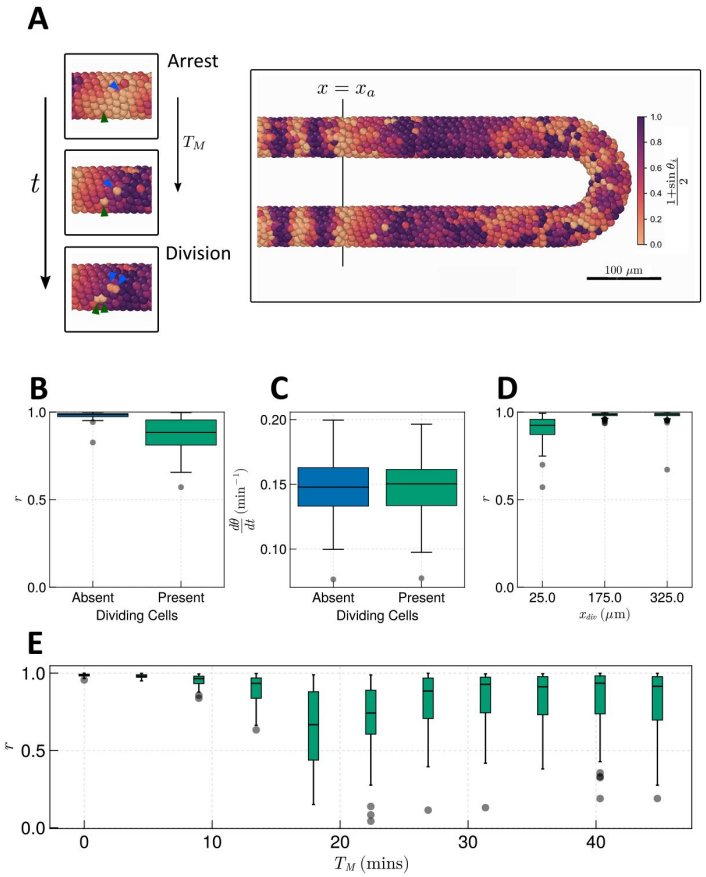

Figure 6—figure supplement 1.

The effect of cell division on frequency. **A** Effect on median frequency when varying x_{div} after 1000 mins for N=100 simulations. **B** Effect on median frequency when varying T_M after 1000 mins for N=100 simulations.

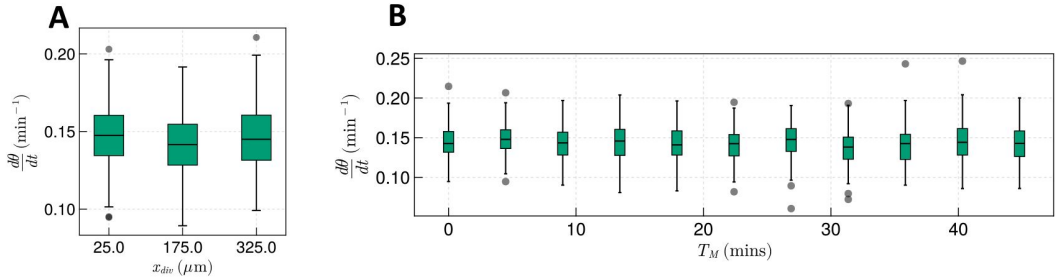

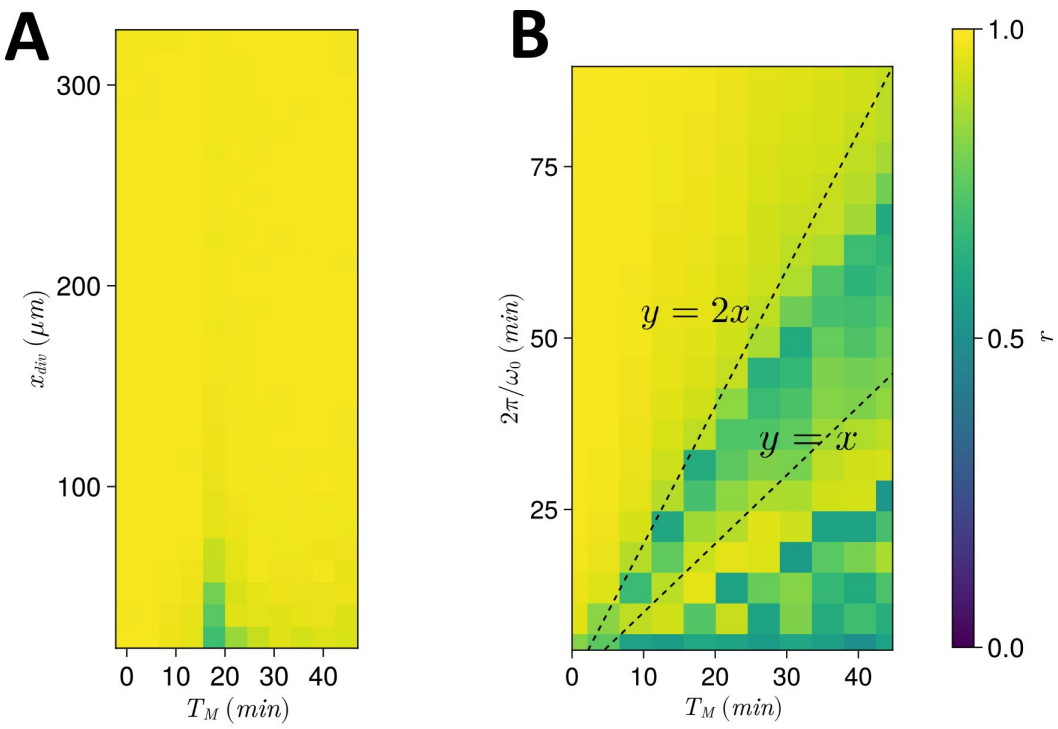

Figure 6—figure supplement 2.

A Dependence of anterior synchrony on x_{div} and T_M. The median anterior synchrony after 1000 mins for N=100 simulations is plotted. **B** Dependence of anterior synchrony on T_M and intrinsic clock frequency ω_0. The median anterior synchrony after 1000 mins for N=100 simulations is plotted.

tissue anterior without a major defect in synchrony (**figure 6** supp 2A). For T_M > 15 mins simulations with division show high synchrony at the anterior although not so high as those with T_M < 15 mins, where the value of x_{div} such that clock synchrony is preserved is displaced to the posterior (**figure 6** supp 2A). However, only for T_M = 15 mins is this value majorly displaced to the posterior, with $x_{div} \approx 150\mu m$ being the anterior-most value of x_{div} such that synchrony is preserved ($r \approx 1$) (figure supp 2A). This result is perhaps intuitive, as the parameters in the model set the clock period to $2\pi/\omega_0$ = 30 mins, and a clock arrest lasting T_M = 15 mins would be sufficient to move a cell into antiphase relative to its neighbours. Indeed we see that mitosis is most deleterious to synchrony when M-phase lasts approximately half the length of a clock cycle (**figure 6** supp 2B), however for long clock cycles this relationship becomes nonlinear and the most deleterious values of T_M lie between the length of one or two clock cycles (**figure 6** supp 2B).

Zebrafish clock coupling and cell mixing confers robustness to changes in cell ingression

Across many of the morphogenetic scenarios tested here, we have observed a high degree of robustness in clock dynamics with respect to changing cell movements and processes. As shown above, some of this robustness can be attributed to the choice of tissue length L in simulations, and choices of the parameters v_a and v_p governing the advection velocity of cells. However we also expect that the rate of cell mixing (Uriu et al. (2010, 2013, 2017)), and the strength of clock coupling, confer robustness too. Within the present model, the global rate of cell mixing is controlled by the parameter v_s and the clock coupling strength is denoted by k. Notably, the values taken for these parameters have been experimentally measured in zebrafish (Riedel-Kruse et al. (2007); Herrgen et al. (2010); Uriu et al. (2017, 2021)). Therefore we were interested in where these parameters lie within the space of parameter pairs that generate clock dynamics robust to changes in morphogenesis - do these results reflect something unique about the zebrafish parameters or can many (κ, v_s) pairs confer robustness?

To determine this, we take changing cell ingression as an example of varying morphogenesis and for each ingression scenario, systematically enumerate the parameters v_s and k, studying the anterior synchrony after 1000 mins with N=100 replicates per parameter pair. This reveals a threshold curve of (κ, v_s) pairs below which the clock begins to exhibit asynchrony (**figure 7**). Comparing across the three scenarios of cell ingression we see that the position of this curve changes with the cell ingression scenario (**figure 7**), indicating that the space of (k, v_s) pairs that achieve clock synchrony is constrained by the cell ingression mode present within the tissue. Notably the experimentally-derived parameter pair ($\kappa = 0.07\ \text{min}^{-1}$, $v_s = 1\ \mu\text{m} \cdot \text{min}^{-1}$) lies very close to the threshold for the DP+LV case of cell ingression in the k direction, suggesting that the robustness we have observed in response to changes in cell ingression is sensitive to the choice of κ. However in each case our experimental choices for κ and v_s lie above the threshold, implying that at least part of the robustness we observed with respect to cell ingression is due to the experimental values for zebrafish being sufficient to confer this robustness.

Discussion

Here we investigated whether morphogenesis of the PSM and the segmentation clock exhibit developmental modularity, as this could explain the high degree of evolvability observed in vertebrate segment number (Raff (1996)). We tested a broad range of PSM cellular behaviours and mechanisms that are associated with the elongation of the PSM across vertebrate species, to see if they had an effect on the dynamics of the segmentation clock. We predict that the dynamics of the zebrafish segmentation clock, specifically synchrony and frequency, are generally robust to changes in these mechanisms such as cell ingression, motility, and (under certain conditions)

Figure 7.

Anterior synchrony after 1000 mins, for varying maximum magnitude of intrinsic cell motion v_s and clock phase coupling strength k, for three different scenarios of cell ingression. Each pixel corresponds to the median value of anterior synchrony across N = 100 simulations. A black + marks the experimental values for zebrafish, $v_s = 1\ \mu\text{m} \cdot \text{min}^{-1}$, $k = 0.07\ \text{min}^{-1}$, derived in Uriu et al. (2017) and Riedel-Kruse et al. (2007) respectively, that are used elsewhere in this paper. All other parameters are held constant at their normal values (see **table 1**).

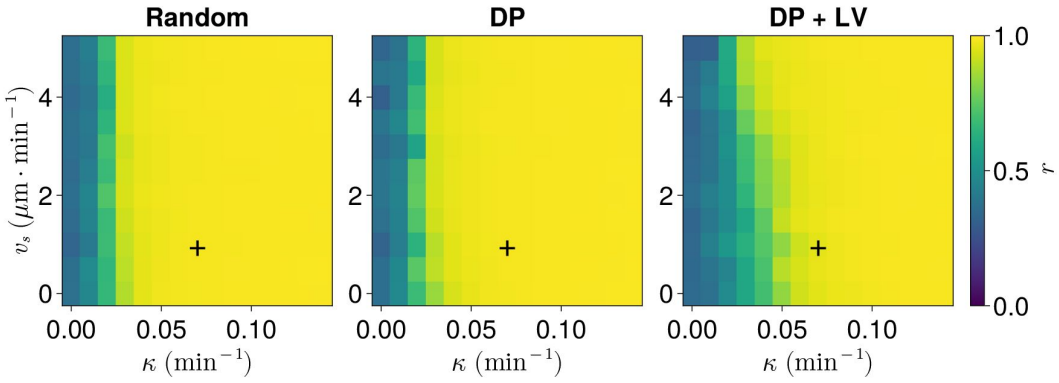

Figure 8.

Top: schematic of the PSM in the xy plane. The PSM is comprised of two cylinders, centred at $y = r$ and $y = 2R + r$, respectively, with radius r. The 'Tailbud' is represented as a half-torus domain centred at $\mathbf{x} = (X_c, Y_c, Z_c)^T$, with internal radius r and radius from torus centre R. Cross-sections of the PSM and Tailbud are highlighted in magenta, and illustrated on the **bottom**, showing how a point within the tissue $\mathbf{x}_i$ is assigned the polar coordinates r_i and q_i. Adapted from Uriu et al. (2021).

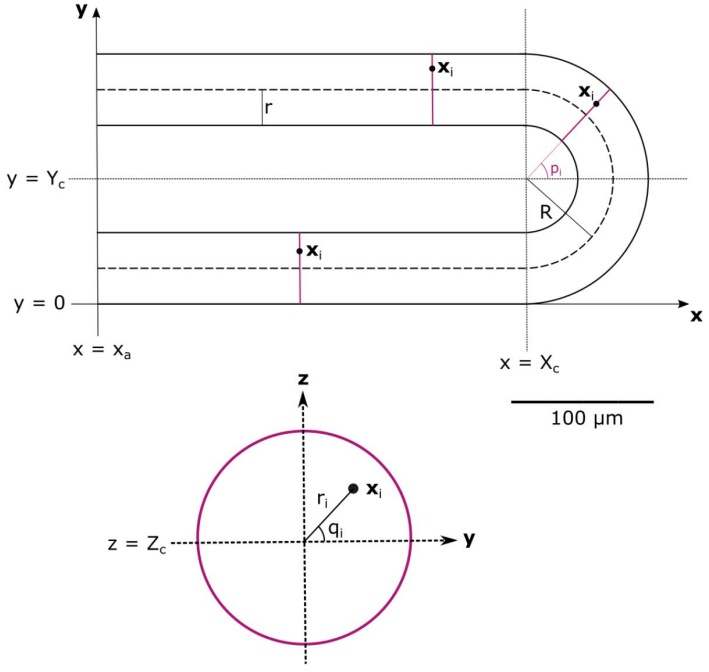

division. As PSM morphogenesis is independent of the clock Schröter et al. (2008); Forero et al. (2018), our results suggest that the clock and morphogenesis of the PSM exhibit developmental modularity.

Our results suggest that a major determinant of this robustness is the clock coupling κ, which in zebrafish appears to be sufficiently strong to confer robustness to changes in cell ingression (**figure 7**). While synchrony of the clock shows a dependence on cell mixing rate (v_s) and tissue length (L), the dependence of synchrony on these parameters is weak compared to its dependence on coupling strength (**figure 7**, **figure 4** supp 1), suggesting that this robustness may be more dependent on properties of the segmentation clock than those of the tissue. Due to a lack of quantitative understanding of PSM morphogenesis, it is difficult to predict whether the requirements for robustness imposed on cell mixing or tissue length and density constrain the space of possible morphogenetic processes that can be altered without perturbing the clock. However, our results highlight that these requirements are themselves constrained by the strength of clock phase-coupling, so it is equally possible that vertebrate segmentation clocks have sufficiently strong phase-coupling generally, and these requirements on morphogenesis are sufficiently relaxed to not constrain the evolution of PSM elongation. Further work, investigating the evolution of phase-coupling strength in vertebrates, and developing accurate quantitative models of PSM morphogenesis, will be necessary to determine this.

It is also worth noting that while in the model formulation κ represents the strength of delta-notch signalling between cells, the experimental value for this parameter is measured at a tissue level, incorporating coupling effects from other pathways e.g. cell mixing (Riedel-Kruse et al. (2007)). It is therefore possible that our choice of κ represents an over-estimate of the strength of delta-notch signalling and, when we combine this with cell mixing in the model, our results present an over-estimate of robustness. However, the precise value of r at which a somite is correctly patterned is unknown, and indeed there exist processes independent of the segmentation clock that can act to correct against inaccuracies in somite length (Naganathan et al. (2022)), so it is plausible that somitogenesis may be more tolerant of clock asynchrony than we suppose here and that somites are correctly patterned for $r < 1$. As our results appear less sensitive to cell mixing (v_s) than κ (**figure 7**), we suggest that the contribution of cell mixing to an experimental estimate of κ may be minor. Therefore, combined with a tolerance of somitogenesis for values of $r < 1$, we suggest that our findings are robust to any overestimates of κ incorporating cell mixing.

Our analysis is restricted to the modes of PSM morphogenesis that are known to occur in vertebrates, and we cannot rule out the possibility that the robustness we observe merely reflects evolution of mechanisms of PSM elongation under selective pressure to minimise their effect on the clock, and that the clock may not be robust to all possible modes of PSM elongation. Nevertheless, we argue that our results demonstrate there exists a qualitatively distinct set of processes (cell ingression, division, motility, and compaction-extension) that underpin PSM elongation and do not affect clock dynamics. As vertebrate species appear to employ a combination of these processes to varying degrees (Bénazéraf et al. (2010); Steventon et al. (2016); Mongera et al. (2018); Xiong et al. (2020); Thomson et al. (2021)), it is possible that evolution alters each of these processes independently to generate diversity in the elongation dynamics of the PSM (Gomez et al. (2008); Steventon et al. (2016)). Therefore this relatively small set of processes may be sufficient to explain the high degree of evolvability in vertebrate segment number.

As clock dynamics appear to be robust to changes in morphogenesis, we suggest that the clock and morphogenesis of the PSM comprise two developmental modules within zebrafish, and that this is true more generally whenever the phase coupling of the clock is sufficiently strong, cell mixing sufficiently rapid, or the PSM sufficiently dense and long. We suggest that this may have contributed to the evolution of broad diversity in vertebrate segment number Richardson et al. (1998), and be a present source of evolvability in vertebrates. We note that the evolution of

modularity is an active area of research (Wagner and Altenberg (1996); Wagner et al. (2007)), and suggest that studying the evolution of delta-notch signalling in vertebrates, and the evolutionary origin of the PSM and somitogenesis, may be an illuminating model paradigm for this field. We predict that the modularity of the clock and morphogenesis of the PSM permits a synergy between these two processes that heightens the evolvability of segment number in vertebrates, and that this may be responsible for the high diversity we observe in this trait (Richardson et al. (1998)).

Methods

Computational model of the segmentation clock and PSM

To simulate the movements of cells within the PSM and the dynamics of the segmentation clock, we used the model of Uriu et al. (2021), who sought to explain defective somite patterning after loss of Notch-Delta signalling (Uriu et al. (2021)). Here an abstract phase oscillator Kuramoto model is used to describe intracellular clock oscillations and cell-cell phase coupling. Cells are confined within a three-dimensional tissue domain whose geometry approximates that of the PSM.

This model is suitable for our purposes because it provides a three-dimensional model of cell movements within the PSM, allowing us to alter morphogenesis in order to test hypotheses. Additionally, as the segmentation clock here is described as an abstract phase oscillator, the model has broad applicability to different vertebrate species which are known to differ in the structure and regulation of their segmentation clock gene regulatory networks (Krol et al. (2011)). Finally, the validity of the model has been shown in several ways via comparison with data for zebrafish (Webb et al. (2016); Liao et al. (2016); Uriu et al. (2021)), and uses parameters experimentally inferred from zebrafish embryos (Riedel-Kruse et al. (2007); Soroldoni et al. (2014); Uriu et al. (2021)). This gives an accurate read-out of the effect of changing morphogenesis on the segmentation clock of a vertebrate.

The model is described elsewhere (Uriu et al. (2021)), but for completeness we include an account of it here. For clarity, vector variables are shown in **bold**, and scalar variables in normal font.

Tissue geometry and frame of reference

The model assumes that the posterior tip of the PSM is held in an inertial frame of reference, and models the posterior-ward elongation of the PSM by movement of cells to-wards the tissue anterior.

Cells are confined within a horseshoe-shaped domain resembling the PSM. This domain is comprised of two cylindrical sub-domains and one half-toroid subdomain, each representing the lateral sides of the PSM and tailbud, respectively. A schematic can be seen in **figure 8**. Cells are free to move between each domain and leave the tissue at the anterior at $x = x_a$.

The centre of the toroid domain is denoted by the coordinate vector $(X_c, Y_c, Z_c)^T$, and the anterior of the PSM is demarcated by the x-coordinate $x = x_a$ (see **figure 8**). The major radius of the torus is denoted by R and the minor radius (and the radius of the two cylindrical domains) is denoted by r (see **figure 8**). The resulting length of the PSM in the x direction, L, is therefore given by $L = r + R + X_c - x_a$.

Cell movement

To approximate cell mixing and the advection of cells out of the PSM towards the anterior (in the chosen tailbud-inertial frame of reference), cell movement in the model is described by an equation of motion that incorporates cell advection, cell-cell repulsion, random cell motion, and a boundary force confining cells within the tissue domain (**Equation (1)**).

Specifically, each cell is assigned a position vector $\mathbf{x}_i \in \mathbb{R}^3$, where $\mathbf{x}_i = (x_i, y_i, z_i)^T$. This position $\mathbf{x}_i$ corresponds to the cell centre. Cells are assumed to be spheres with diameter d_c. The equation of motion for cell i is

$$\frac{\mathrm{d}\mathbf{x}_i}{\mathrm{d}t} = \mathbf{v}_d(x_i) + v_0(x_i)\mathbf{n}_i(t) + \sum_{j=1, j\neq i}^{N} \mathbf{F}(\mathbf{x}_i, \mathbf{x}_j) + \mathbf{F}_b(\mathbf{x}_i), \tag{1}$$

where $\mathbf{v}_d(x_i)$ represents the advection of the cell towards the PSM anterior, $v_0(x_i)\mathbf{n}_i(t)$ the intrinsic random motion of the cell, $\mathbf{F}(\mathbf{x}_i, \mathbf{x}_j)$ the repulsion force between cell i and cell j, and $\mathbf{F}_b(\mathbf{x}_i)$ the boundary force confining the cell within the tissue.

The advection velocity $\mathbf{v}_d(x_i)$ is given by

$$\mathbf{v}_d(x_i) = (-v_d(x_i), 0, 0)^T, \tag{2}$$

where the function $v_d(x_i)$ describes the local strain rate along the AP axis:

$$v_d(x_i) = \begin{cases} -\frac{v_a - v_p(1-x_q)}{x_q} \cdot \frac{x_i - x_a}{L} + v_a & \frac{x_i - x_a}{L} \leq x_q, \\ -\frac{v_p(x_i - x_a)}{L} + v_p & \frac{x_i - x_a}{L} > x_q, \end{cases} \tag{3}$$

The model assumes that the random cell motility observed within the PSM is intrinsic, i.e. cells would exhibit random motility in isolation from the tissue. This is modelled using the direction vector $\mathbf{n}_i(t)$, which evolves according a random walk on the surface of the unit sphere specified by the following differential equation:

$$\frac{\mathrm{d}\mathbf{n}_i}{\mathrm{d}t} = \sqrt{2D}\xi_{\phi_i}(t)\mathbf{m}_x + \sqrt{2D}\xi_{\varphi_i}(t)\mathbf{m}_y - 2D\mathbf{n}_i(t), \tag{4}$$

where the orthogonal vectors (for $\mathbf{e}_z = (0, 0, 1)^T$)

$$\mathbf{m}_x = \frac{\mathbf{n}_i(t) \times \mathbf{e}_z}{|\mathbf{n}_i(t) \times \mathbf{e}_z|}, \ \mathbf{m}_y = \frac{\mathbf{m}_x \times \mathbf{n}_i(t)}{|\mathbf{m}_x \times \mathbf{n}_i(t)|}, \tag{5}$$

together define a plane tangent to the unit sphere, and $\xi_\varphi(t)$, $\xi_\phi(t)$ are white Gaussian noise terms that satisfy, for any t, t', $\langle \xi_{\phi_i}(t) \rangle = \langle \xi_{\varphi_i}(t) \rangle = \langle \xi_{\phi_i}(t)\xi_{\varphi_j}(t) \rangle = 0$, and $\langle \xi_{\phi_i}(t)\xi_{\phi_j}(t) \rangle = \langle \xi_{\varphi_i}(t)\xi_{\varphi_j}(t) \rangle = \delta_{ij}\delta(t - t')$. A derivation for **equation (4)** is given by Uriu et al. (2021).

To model the increase in random cell motion towards the PSM posterior, the magnitude of intrinsic random cell movement, $v_0(x)$, increases towards the posterior according to equation (6):

$$v_0(x_i) = \frac{v_s}{1 + (\frac{1 - \frac{x_i - x_a}{L}}{X_v})^h}, \tag{6}$$

The parameters v_s, X_v, and h determine the maximum magnitude of intrinsic cell motion, profile inflexion point, and steepness of the profile, respectively. By varying these parameters one can create a variety of motility profiles with different shapes and amplitudes (see **figure 3B**). Here the x-position of cell i is normalised according to the length of the PSM L, and so the profile of cell motility scales with the length of the PSM. This is a valid assumption as the length of the PSM is thought to be partially specified by FGF signalling (Simsek and Özbudak (2018)), and the random motility of PSM cells is also under the control of FGF (Bénazéraf et al. (2010)).

Cell-cell repulsion is encoded by repulsion of two cells if their centres are within a cell diameter d_c of one another, according to the cell-cell repulsion force $\mathbf{F}(\mathbf{x}_j - \mathbf{x}_i)$:

$$\mathbf{F}(\mathbf{x}_j - \mathbf{x}_i) = F(\mathbf{x}_j - \mathbf{x}_i)\frac{\mathbf{x}_j - \mathbf{x}_i}{|\mathbf{x}_j - \mathbf{x}_i|}, \tag{7}$$

where the magnitude of the cell-cell repulsion force $F(\mathbf{x}_j - \mathbf{x}_i)$ is given by

$$F(\mathbf{x}_j - \mathbf{x}_i) = \begin{cases} \mu(\frac{|\mathbf{x}_j - \mathbf{x}_i|}{d_c} - 1) & |\mathbf{x}_j - \mathbf{x}_i| \le d_c, \\ 0, & |\mathbf{x}_j - \mathbf{x}_i| > d_c \end{cases} \tag{8}$$

and the parameter μ controls the strength of cell-cell repulsion throughout the tissue. For computational simplicity, cell-cell adhesion is not encoded within this model.

The form of the boundary force $\mathbf{F}_b(\mathbf{x}_i)$ varies depending on whether the cell i is in one of the lateral PSM cylindrical domains or in the half-toroid tailbud (**figure 8**). If cell i lies within the cylinders, one can use the cylindrical coordinates for cell i, r_i and q_i (see **figure 8**) to naturally define the boundary force:

$$\mathbf{F}_b(\mathbf{x}_i) = \begin{pmatrix} 0 \\ -\mu_b e^{-\frac{\delta y}{r_b}} \cos q_i \\ -\mu_b e^{-\frac{\delta z}{r_b}} \sin q_i \end{pmatrix}, \tag{9}$$

where

$$\delta y = |(r - r_i)\cos q_i|, \tag{10}$$

$$\delta z = |(r - r_i)\sin q_i|, \tag{11}$$

The magnitude of the boundary force is denoted by μ_b and the parameter r_b determines the length-scale of the boundary force. In the half-toroid tailbud the position $\mathbf{x}_i$ of each cell i can be described according to the coordinates r_i, p_i, and q_i:

$$\mathbf{x}_i = \begin{pmatrix} X_c + R\cos p_i + r_i \cos p_i \cos q_i \\ Y_c + R\sin p_i + r_i \sin p_i \cos q_i \\ Z_c + r_i \sin q_i \end{pmatrix}, \tag{12}$$

One can then naturally define

$$\delta x = |(r - r_i)\cos p_i \cos q_i|, \tag{13}$$

$$\delta y = |(r - r_i)\sin p_i \cos q_i|, \tag{14}$$

$$\delta z = |(r - r_i)\sin q_i|, \tag{15}$$

describing the distance of cell i from the tissue surface in the x, y, and z directions, respectively. The boundary force then becomes

$$\mathbf{F}_b(\mathbf{x}_i) = \begin{pmatrix} -\mu_b e^{-\frac{\delta x}{r_b}} \cos p_i \cos q_i \\ -\mu_b e^{-\frac{\delta y}{r_b}} \sin p_i \cos q_i \\ -\mu_b e^{-\frac{\delta z}{r_b}} \sin q_i \end{pmatrix}, \tag{16}$$

Note that in both definitions of $\mathbf{F}_b(\mathbf{x}_i)$, the tissue domains are open-ended, i.e. cells are free to move between subdomains, and out of the PSM at the anterior.

For further details we direct the reader to consult Uriu et al. (2021).

Cell addition

As cells are removed from the tissue by advection, new cells must be added to replenish the PSM. Loss of cells is monitored by comparing the total density of cells in each of the subdomains with a target density, ρ_0. If the density in any of these subdomains falls below ρ_0, a new cell is added to that domain. If the density of more than one of the domains falls below ρ_0 then a cell is only added to the subdomain with the lowest density. The position and phase of the nascent cell both vary across different simulations discussed here. Below is a description of how these quantities vary.

In simulations where cell addition is 'Random', cells are added with a random position within each domain, with a random phase, i.e. if a cell is added within one of the cylindrical domains, it is given a random $x_i \in [x_a + x_d, X_c]$, a random $r_i \in [0, r]$, and $q_i \in [0, 2\pi)$. Alternatively, if the cell is added within the half-toroid domain, it is given a random $p_i \in [-\pi/2, \pi/2]$, and random r_i and q_i, defined as above. The cell is also assigned a random phase $\theta_i \in [0, 2\pi)$. This method of cell addition is unbiased in terms of its effect on the model but is a biologically implausible scenario of cell ingression, so we use it here as a negative control.

In simulations where we seek to more accurately model cell ingression, cells are added on the cell surface, i.e. $r_i = r$. Additionally, the surface domain on which cells can be added is restricted. For the half-toroid domain, we restrict cell addition to the dorsal quarter of the domain, i.e. $q_i \in [\pi/4, 3\pi/4]$, $p_i \in [-\pi/2, \pi/2]$. For the cylindrical domains we restrict addition to the bottom quarter of the surface, i.e. $q_i \in [5\pi/4, 7\pi/4]$. To more accurately model conditions of cell ingression combinations of these three modes of cell addition are employed (**figure 2**).

In newly added cells the direction vector $\mathbf{n}$ is initialised with a random vector of unit length. For simulations where cell division is present, cells are added with a random cell cycle phase $\tau \in 0, T_G + T_M$.

Coupled oscillator model of the segmentation clock

Here only the phase of each cell's segmentation clock cycle is considered, and oscillation amplitudes are neglected. This simplification is appropriate when oscillator coupling is weak (Kuramoto (1984)). Here oscillators have a spatially-dependent intrinsic frequency $\omega(x_i)$, and

couple to adjacent cells (defined as those within d_c, a cell's diameter) with a magnitude controlled by the scalar value κ:

$$\frac{d\theta_i}{dt} = \omega(x_i) + \frac{\kappa}{N_i(t)} \sum_{|\mathbf{x}_j - \mathbf{x}_i| \le d_c} \sin(\theta_j - \theta_i) + \sqrt{2D_\theta}\xi_{\theta_i}(t), \tag{17}$$

Oscillations are noisy, with phase noise intensity D_θ. $\xi_{\theta_i}(t)$ is a Gaussian noise term with $\langle \xi_{\theta_i}(t) \rangle = 0$, $\langle \xi_{\theta_i}(t)\xi_{\theta_j}(t') \rangle = \delta_{ij}\delta(t - t')$ for all t, t'. $N_i(t)$ is the number of cells within a radius of length d_c of cell i at time t, i.e. $N_i(t) = |\{j \mid |\mathbf{x}_j(t) - \mathbf{x}_i(t)| \le d_c\}|$.

The intrinsic frequency $\omega(x_i)$ decreases toward the PSM anterior, creating a frequency gradient and travelling phase waves that move toward the anterior (Soroldoni et al. (2014)). $\omega(x_i)$ is defined as:

$$\omega(x_i) = \omega_0\left(\sigma + (1 - \sigma) \cdot \frac{1 - e^{-\frac{k(x - x_a)}{L}}}{1 - e^{-k}}\right), \tag{18}$$

where ω_0 corresponds to the frequency of cells at the posterior of the tissue, σ the fold-change in frequency at the anterior compared to the posterior, and κ controls the shape of the gradient.

To simulate the effect of the wavefront, where the clock phase is interpreted by cells to pre-pattern somite boundaries (Cooke and Zeeman (1976)), beyond $x = x_a$ oscillations arrest, forming stable patterns of phase (**figure 2A**), i.e. $d\theta_i/dt = 0$ if $x_i < x_a$.

Cell division and segmentation clock arrest

During M phase of the cell cycle, the segmentation clock arrests (Horikawa et al. (2006); Delaune et al. (2012)). To simulate this, we assign each cell i a cell cycle phase $\tau \in [0, T_G + T_M)$, where T_G and T_M are the duration of G1-G2 and M phases in minutes respectively, and evolve τ according to

$$\tau = (t - t_{addition}) \mod (T_G + T_M), \tag{19}$$

where $t_{addition}$ denotes the time at which the cell was added.

To simulate the arrest of segmentation clock gene expression during M phase of the clock, we evolve θ_i according to

$$\frac{d\theta_i}{dt} = H(T_G - \tau_i) \cdot \left(\omega(x_i) + \frac{\kappa}{N_i(t)} \sum_{|\mathbf{x}_j - x_i| \le d_c} \sin(\theta_j - \theta_i) + \sqrt{2D_\theta}\xi_{\theta_i}(t)\right), \tag{20}$$

where $H(x)$ is the Heaviside step function:

$$H(x) = \begin{cases} 1 & x > 0, \\ 0 & x \le 0, \end{cases} \tag{21}$$

If $\tau_i \ge T_G + T_M$ then we consider the cell cycle complete and a new cell κ is added at a random position of length d_{new} away from cell i, i.e.

$$\mathbf{x}_k = \mathbf{x}_i + d_{new}\begin{pmatrix} \cos\varphi \sin\phi \\ \sin\varphi \sin\phi \\ \cos\phi \end{pmatrix},$$

for uniformly distributed random $\varphi \in [0, \pi]$, $\phi \in [0, 2\pi)$. Other variables are inherited from cell i, i.e. $n_\kappa = n_i$ and $\theta_\kappa = \theta_i$. The choice of d_{new} is somewhat arbitrary, however as this distance decreases the magnitude of the cell-cell repulsion force (equation (8)) grows very large, and one must choose a d_{new} sufficiently small to be biologically accurate while large enough to avoid implausible cell velocities due to a very large cell-cell repulsion force. We find that $d_{new} = d_c/10$ is a suitable compromise between these two scenarios.

We are not aware of any direct measurements of T_G within the zebrafish PSM, and so have calculated a value for this parameter based on some assumptions. M phase within the PSM lasts approximately 15 mins, and approximately 8% of cells in the PSM at a single time point are in M phase (Horikawa et al. (2006); Kanki and Ho (1997)). Cells in M phase appear to be distributed homogenously in space (Kanki and Ho (1997)), and there-fore cell cycles in the PSM may be independent, in which case the total duration $T_G + T_M$ is approximately equal to 15/0.08 = 187.5 mins, and T_G = 172.5 mins. Unless otherwise stated, we fix $T_G + T_M = 187.5$.

Modelling compaction-extension

To model the compaction-extension of the PSM (Thomson et al. (2021)), we shrink the PSM radius r, and length L over time, concurrent with an increase in density ρ_0 and a step-wise decrease in cell diameter d_c (see **figure 5**). This is derived from the observations of Thomson et al. (2021) who observed changes in the PSM height, width, length, density, and cell diameter, during the latter stages of zebrafish somitogenesis. We sought to model this process using the rates of change in these parameters described by Thomson et al. (2021), however as their published rates are in units of change per somite stage, and the rate of somitogenesis is nonlinear in zebrafish (Schröter et al. (2008)), we needed an interpolation of somite number over time in order to describe the according change in rate over time.

To this, we extracted the data for somite number over time from Schröter et al. (2008) using the web app WebPlotDigitizer (Rohatgi (2022)), and fitted a function of the form

$$s(t) = 6 + \frac{t}{24.7} - ae^{b(t-300)}, \tag{22}$$

for unknown parameters a, b, using the Julia package LsqFit.jl. We obtained values of $a = 0.5001$ and $b = 0.0049$ using this process. Using this interpolation of somite number over time, we then could change the tissue radius, length, cell diameter, and density, using the values published in Thomson et al. (2021). As this only occurs in the latter stages of somitogenesis (measured only from 16ss onwards), we hold these variables constant before the time at which 16 somites are formed in zebrafish.

The equations describing change in tissue length (L), wavefront position (x_a), and anterior limit of cell addition therefore become:

$$L(t) = \begin{cases} L_0 & s(t) < 16, \\ L_0 - m_a(s(t) - 16) & s(t) \geq 16, \end{cases} \tag{23}$$

$$x_a(t) = \begin{cases} x_{a0} & s(t) < 16, \\ x_{a0} + m_a(s(t) - 16) & s(t) \geq 16, \end{cases} \tag{24}$$

$$x_d(t) = x_a(t) + 100, \tag{25}$$

where m_a denotes the rate at which the PSM shrinks in length, and L_0 and x_{a0} the initial values for L and x_a before shrinking, respectively. The equation describing the change in radius r is

$$r(t) = \begin{cases} r_0 & s(t) < 16, \\ r_0 - m_r(s(t) - 16) & s(t) \geq 16, \end{cases} \tag{26}$$

where m_r denotes the rate at which the PSM shrinks in radius, and r_0 the initial value for r before shrinking. In their work Thomson et al. (2021) reported that the PSM shrinks in height more rapidly at the PSM posterior than at the anterior, however the rate of shrinkage of the PSM in width (along the medio-lateral axis) was the same across the anterior and posterior halves of the PSM (Thomson et al. (2021)). As our model assumes the tissue is as wide as it is tall, we take only the rate of shrinkage in the medio-lateral axis in our value for m_r, and calculate m_r by taking the mean of the two (similar) rates published by Thomson et al. (2021) for the anterior and posterior halves of the PSM.

The functions describing change in tissue density ρ and cell diameter d_c are similarly

$$\rho(t) = \begin{cases} \rho_{t0} & s(t) < 16, \\ \rho_{t0} + m_\rho(s(t) - 16) & s(t) \geq 16, \end{cases} \tag{27}$$

and

$$d_c(t) = \begin{cases} d_{c0} & s(t) < 16, \\ d_{c0} - m_{d_c}(s(t) - 16) & s(t) \geq 16, \end{cases} \tag{28}$$

where m_ρ and m_{d_c} represent the rates of change in density and cell diameter, respectively, and ρ_{t0} and d_{c0} the initial values for density and cell diameter, respectively, before shrinking. In their work Thomson et al. (2021) only report the cell diameter for 16ss and 26ss zebrafish embryos, but we choose to shrink the diameter of cells at the rate they describe, measured between these two timepoints. Our results are insensitive to choice of a function for d_c (t) where cells continue shrinking in diameter at the same rate past 26ss, or not (see **figure 5** supp 1).

Initial conditions

To initialise the simulation, N cells are generated with random positions

$$\mathbf{x}_i = \begin{pmatrix} x_i \\ r + r_i \cos q_i \\ Z_c + r_i \sin q_i \end{pmatrix},$$

and a further N with positions

$$\mathbf{x}_i = \begin{pmatrix} x_i \\ r + 2R + r_i \cos q_i \\ Z_c + r_i \sin q_i \end{pmatrix},$$

and then a further N_{TB} with positions

$$\mathbf{x}_i = \begin{pmatrix} X_c + R\cos p_i + r_i \cos p_i \cos q_i \\ Y_c + R\sin p_i + r_i \sin p_i \cos q_i \\ Z_c + r_i \sin q_i \end{pmatrix},$$

for $x_i \in [x_a, X_c]$, $p_i \in [-\pi/2, \pi/2]$, $q_i \in [0, 2\pi]$, and $r_i \in [0, r]$, where $N = \lfloor \rho_0 \pi r^2 X_c \rfloor$ and $N_{TB} = \lfloor \rho_0 \pi^2 r^2 R \rfloor$. As this generates more cells near the tissue mid-line than at the periphery, in order to homogenise local density the tissue is 'relaxed' for 10 mins, whereby $\mathbf{x}_i$ evolves according to

$$\frac{\mathrm{d}\mathbf{x}_i}{\mathrm{d}t} = v_0(x_i)\mathbf{n}_i(t) + \sum_{j=1, j\neq i}^{N} \mathbf{F}(\mathbf{x}_i, \mathbf{x}_j) + \mathbf{F}_b(\mathbf{x}_i), \tag{29}$$

and $\mathbf{n}_i(t)$ evolves according to equation (4). This causes cells to be evenly distributed throughout the tissue.

When cells are initialised prior to relaxation, $n_i(t)$ is assigned for each cell at random, i.e. $\mathbf{n}_i(0) = (\cos\phi_i \sin\varphi_i, \sin\phi_i \sin\varphi_i, \cos\varphi_i)^T$ for random $\phi_i \in [0, 2\pi)$, $\varphi_i \in [0, \pi]$. The segmentation clock phase θ_i is also assigned as a constant value $\theta_i(0) = 3\pi/2$.

Parameter values

Parameter values, and their source, are shown in **Table 1**.

Implementation

Equations 1 and 17 are solved from the initial conditions outlined above across a 1000 min time-span using an forward Euler scheme in Julia v1.8.2, using a time step $dt = 0.01$ mins. Code for simulation and analysis can be found at *https://github.com/jewh/ModularityPSMClock*.

Analysis and metrics

Here we measure clock dynamics using two metrics. The first is the synchrony of the segmentation clock across cells, denoted r, calculated by

$$re^{i\psi} = \frac{1}{N}\sum_{j=1}^{N} e^{i\theta_j}, \tag{30}$$

which is sometimes referred to as the Kuramoto phase order parameter. When $r \approx 0$, oscillations are asynchronous, and when $r \approx 1$, oscillations are synchronous.

The second metric is the average (mean) frequency of cells in a given domain, where the frequency $\mathrm{d}\theta/\mathrm{d}t$ is simply the value of *equation 17*. In cases where we are interested in changes in frequency upon varying model parameters, we find it convenient to define

$$\Delta\frac{\mathrm{d}\theta}{\mathrm{d}t} = \frac{\mathrm{d}\theta}{\mathrm{d}t} - \frac{1}{d_c}\int_{x_a}^{x_a+d_c} \omega(x)\mathrm{d}x, \tag{31}$$

in order to highlight changes in frequency.

In order to analyse the output of a simulation in terms of one value, for many analyses we calculate r, $\mathrm{d}\theta/\mathrm{d}t$, or $\Delta\mathrm{d}\theta/\mathrm{d}t$, for the cells within one cell's diameter of the anterior (i.e. $x_a \leq x_i \leq x_a + d_c$). We do this because at the wavefront oscillations arrest and pre-pattern somites, and

Symbol	Value	Units	Symbol	Value	Units
X_c	300	μm	L	$X_c - x_a + R + r$	μm
Y_c	85	μm	x_a	0	μm
Z_c	25	μm	x_d	100	μm
R	60	μm	x_q	0.7	-
r	25	μm	d_c	11	μm
v_a	1.67	μm·min^{-1}	D	0.026	min^{-1}
v_p	3	μm·min^{-1}	μ	8.71	μm·min^{-1}
X_v	0.4	-	μ_b	20	μm·min^{-1}
h	3	-	r_b	1	μm
v_s	1	μm·min^{-1}	ρ_0	0.0015	μm^{-3}
L_0	325	μm	T_G	187.5 - 15	min
m_a	14.1	μm ·somite^{-1}	T_M	15	min
r_0	27.6	μm	κ	0.07	min^{-1}
m_r	1.1625	μm ·somite^{-1}	ω_0	0.2094	min^{-1}
d_{c0}	9.2	μm	σ	0.66	-
$m_{d_{c0}}$	0.2	μm ·somite^{-1}	k	3.07	-
ρ_{t0}	0.002123	μm^{-3}	$D\theta$	0.0013	min^{-1}
m_ρ	0.000121	μm ·somite^{-1}			

Table 1.

Parameter values used in our work, unless otherwise stated. Values derived from Kanki and Ho (1997); Horikawa et al. (2006); Riedel-Kruse et al. (2007); Uriu et al. (2017, 2021), and Thomson et al. (2021).

therefore the frequency and synchrony of oscillations immediately adjacent to the PSM anterior will determine the somite length and precision of pre-patterning. We thus regard the values of r, $\mathrm{d}\theta/\mathrm{d}t$, and $\Delta\mathrm{d}\theta/\mathrm{d}t$ as proxies for phenotype exhibited by the simulation. As discussed above, unless stated otherwise we measure clock dynamics after 1000 mins, as we find this sufficient to ensure that the dynamics of the clock have reached a steady state that we deem would be reached in vivo (see **figure 9**).

Acknowledgements

We thank Koichiro Uriu for his help in providing code and first establishing the model. We thank Usha Kadiyala for her comments regarding estimates for T_G. We thank Ben Steventon for his feedback on the project. The authors would like to acknowledge the use of the University of Oxford Advanced Research Computing (ARC) facility in carrying out this work. *http://dx.doi.org/10.5281/zenodo.22558*. This work was supported by a grant from the Simons Foundation (MP-SIP-00001828, REB).

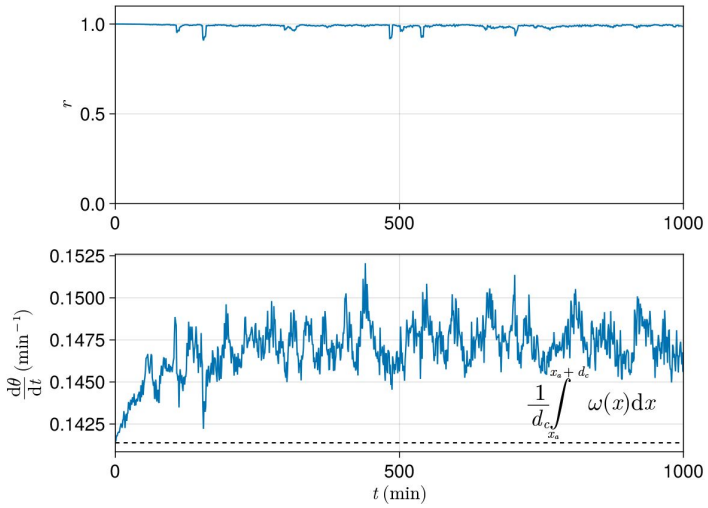

Figure 9.

Top Trace of synchrony r for a d_c -wide domain of cells at the left-hand anterior edge of the PSM over 1000 mins. Data drawn from a single simulation with random cell addition, using parameters as per Uriu et al. (2021). **Bottom** Trace of mean frequency $d\theta/dt$ for a d_c -wide domain of cells at the left-hand anterior edge of the PSM over 1000 mins. Data drawn from the same simulation as above. Plotted with a black dashed line is the average intrinsic frequency $\omega(x)$ across the domain, calculated using the formula shown.

References

Banavar SP, Carn EK, Rowghanian P, Stooke-Vaughan G, Kim S, Campàs O 2021) **Mechanical control of tissue shape and morphogenetic flows during vertebrate body axis elongation** *Scientific reports* **11**:1–14 https://doi.org/10.1038/s41598-021-87672-3

Bouldin CM, Snelson CD, Farr GH, Kimelman D. 2014) **Restricted expression of cdc25a in the tailbud is essential for formation of the zebrafish posterior body** *Genes Development* **28**:384–395 https://doi.org/10.1101/gad.233577.113

Bénazéraf B, Francois P, Baker RE, Denans N, Little CD, Pourquié O 2010) **A random cell motility gradient downstream of FGF controls elongation of an amniote embryo** *Nature* **466**:248–52 https://doi.org/10.1038/nature09151

Cooke J, Zeeman EC 1976) **A clock and wavefront model for control of the number of repeated structures during animal morphogenesis** *Journal of Theoretical Biology* **58**:455–476 https://doi.org/10.1016/s0022-5193(76)80131-2

Delaune EA, François P, Shih NP, Amacher SL 2012) **Single-cell-resolution imaging of the impact of Notch signaling and mitosis on segmentation clock dynamics** *Developmental cell* **23**:995–1005 https://doi.org/10.1016/j.devcel.2012.09.009

Forero LL, Narayanan R, Huitem LF, VanBergen M, Apschner A, Peterson-Maduro J, Logister I, Valentin G, Morelli LG, Oates AC, Schulte-Merker S. 2018) **Segmentation of the zebrafish axial skeleton relies on notochord sheath cells and not on the segmentation clock** *eLife* **7** https://doi.org/10.7554/eLife.33843

Gomez C, zbudak EM, Wunderlich J, Baumann D, Lewis J, Pourquié O 2008) **Control of segment number in vertebrate embryos** *Nature* **454**:335–339 https://doi.org/10.1038/nature07020

Gomez C, Pourquié O 2009) **Developmental control of segment numbers in vertebrates** *Journal of Experimental Zoology Part B: Molecular and Developmental Evolution* **312**:533–544 https://doi.org/10.1002/jez.b.21305

Harima Y, Takashima Y, Ueda Y, Ohtsuka T, Kageyama R. 2013) **Accelerating the Tempo of the Segmen-tation Clock by Reducing the Number of Introns in the Hes7 Gene** *Cell Reports* **3**:1–7 https://doi.org/10.1016/j.celrep.2012.11.012

Herrgen L, Ares S, Morelli LG, Schroter C, Julicher F, Oates AC 2010) **Intercellular Coupling Regulates the Period of the Segmentation Clock** *Current Biology* **20** https://doi.org/10.1016/j.cub.2010.06.034

Horikawa K, Ishimatsu K, Yoshimoto E, Kondo S, Takeda H. 2006) **Noise-resistant and synchronized oscillation of the segmentation clock** *Nature* **441**:719–723 https://doi.org/10.1038/nature04861

Kanki JP, Ho RK 1997) **The development of the posterior body in zebrafish** *Development* **124**:881–893 https://doi.org/10.1242/dev.124.4.881

Krol AJ, Roellig D, Dequéant ML, Tassy O, Glynn E, Hattem G, Mushegian A, Oates AC, Pourquié O 2011) **Evolutionary plasticity of segmentation clock networks** *Development* **138**:2783–2792 https://doi.org/10.1242/dev.063834

Kuramoto Y. 1984) **Chemical turbulence** In: *Chemical oscillations, waves, and turbulence* Springer pp. 111–140

Lawton AK, Nandi A, Stulberg MJ, Dray N, Sneddon MW, Pontius W, Emonet T, Holley SA 2013) **Regulated tissue fluidity steers zebrafish body elongation** *Development* **140**:573–582 https://doi.org/10.1242/dev.090381

Lewis J. 2003) **Autoinhibition with transcriptional delay: A simple mechanism for the zebrafish somitoge-nesis oscillator** *Current Biology* **13**:1398–1408 https://doi.org/10.1016/s0960-9822(03)00534-7

Liao BK, Jörg DJ, Oates AC 2016) **Faster embryonic segmentation through elevated Delta-Notch signalling** *Nature Communications* **7**:1–12 https://doi.org/10.1038/ncomms11861

Mara A, Schroeder J, Chalouni C, Holley SA 2007) **Priming, initiation and synchronization of the segmen-tation clock by deltaD and deltaC** *Nature cell biology* **9**:523–530 https://doi.org/10.1038/ncb1578

Michaut A, Mongera A, Gupta A, Serra M, Rigoni P, Lee JG, Duarte F, Hall AR, Mahadevan L, Guevorkian K, Pourquié O 2022) **Activity-driven extracellular volume expansion drives vertebrate axis elongation** *bioRxiv* https://doi.org/10.1101/2022.06.27.497799

Mongera A, Rowghanian P, Gustafson HJ, Shelton E, Kealhofer DA, Carn EK, Serwane F, Lucio AA, Giammona J, Campàs O 2018) **A fluid-to-solid jamming transition underlies vertebrate body axis elon-gation** *Nature* **561**:401–405 https://doi.org/10.1038/s41586-018-0479-2

Morin-Kensicki EM, Melancon E, Eisen JS 2002) **Segmental relationship between somites and vertebral column in zebrafish** *Development* **129** https://doi.org/10.1242/dev.129.16.3851

Murray PJ, Maini PK, Baker RE 2013) **Modelling oscillator synchronisation during vertebrate axis seg-mentation** In: *Pattern Formation in Morphogenesis* Springer pp. 95–105 https://doi.org/10.1007/978-3-642-20164-6_9

Murray PJ, Carrieri FA, Dale JK 2019) **Cell cycle regulation of oscillations yields coupling of growth and form in a computational model of the presomitic mesoderm** *Journal of Theoretical Biology* **481** https://doi.org/10.1016/j.jtbi.2019.05.006

Naganathan SR, Popovic M, Oates AC 2022) **Left–right symmetry of zebrafish embryos requires somite surface tension** *Nature* **605**:516–521 https://doi.org/10.1038/s41586-022-04646-9

Oates AC, Morelli LG, Ares S. 2012) **Patterning embryos with oscillations: structure, function and dy-namics of the vertebrate segmentation clock** *Development* **139**:625–639 https://doi.org/10.1242/dev.063735

Palmeirim I, Henrique D, Ish-Horowicz D, Pourquié O 1997) **Avian hairy gene expression identifies a molecular clock linked to vertebrate segmentation and somitogenesis** *Cell* **91**:639–648 https://doi.org/10.1016/s0092-8674(00)80451-1

Raff RA 1996) **The Shape of Life – Genes, Development and Evolution of Animal Forms** University of Chicago Press

Richardson MK, Allen SP, Wright GM, Raynaud A, Hanken J. 1998) **Somite number and vertebrate evolu-tion** *Development* **125**:151–160 https://doi.org/10.1242/dev.125.2.151

Riedel-Kruse IH, Müller C, Oates AC 2007) **Synchrony dynamics during initiation, failure, and rescue of the segmentation clock** *Science* **317**:1911–1915 https://doi.org/10.1126/science.1142538

Rohatgi A 2022) **Webplotdigitizer: Version 4.6** https://automeris.io/WebPlotDigitizer

Schröter C, Herrgen L, Cardona A, Brouhard GJ, Feldman B, Oates AC 2008) **Dynamics of zebrafish somitogenesis** *Developmental dynamics: an official publication of the American Association of Anatomists* **237**:545–553 https://doi.org/10.1002/dvdy.21458

Schröter C, Ares S, Morelli LG, Isakova A, Hens K, Soroldoni D, Gajewski M, Jülicher F, Maerkl SJ, Deplancke B, Oates AC 2012) **Topology and dynamics of the zebrafish segmentation clock core circuit** *PLOS Biology* **10**:1–20 https://doi.org/10.1371/journal.pbio.1001364

Schröter C, Oates AC 2010) **Segment number and axial identity in a segmentation clock period mutant** *Current Biology* **20**:1254–1258 https://doi.org/10.1016/j.cub.2010.05.071

Simsek MF, Chandel AS, Saparov D, Zinani OQ, Clason N, zbudak EM 2023) **Periodic inhibition of Erk activity drives sequential somite segmentation** *Nature* **613**:153–159 https://doi.org/10.1038/s41586-022-05527-x

Simsek MF, zbudak EM 2018) **Spatial fold change of FGF signaling encodes positional information for segmental determination in zebrafish** *Cell reports* **24**:66–78 https://doi.org/10.1016/j.celrep.2018.06.023

Soroldoni D, Jörg DJ, Morelli LG, Richmond DL, Schindelin J, Jülicher F, Oates AC 2014) **A Doppler effect in embryonic pattern formation** *Science* **345**:222–225 https://doi.org/10.1126/science.1253089

Steventon B, Duarte F, Lagadec R, Mazan S, Nicolas JF, Hirsinger E. 2016) **Species-specific contribution of volumetric growth and tissue convergence to posterior body elongation in vertebrates** *Development* **143**:1732–1741 https://doi.org/10.1242/dev.126375

Thomson L, Muresan L, Steventon B. 2021) **The zebrafish presomitic mesoderm elon-gates through compaction-extension** *Cells & development* **168**:203748 https://doi.org/10.1016/j.cdev.2021.203748

Uriu K, Ares S, Oates AC, Morelli LG 2013) **Dynamics of mobile coupled phase oscillators** *Physical ReviewE* **87**:032911 https://doi.org/10.1103/PhysRevE.87.032911

Uriu K, Bhavna R, Oates AC, Morelli LG 2017) **A framework for quantifcation and physical modeling of cell mixing applied to oscillator synchronization in vertebrate somitogenesis** *Biology open* **6**:1235–1244 https://doi.org/10.1242/bio.025148

Uriu K, Liao BK, Oates AC, Morelli LG 2021) **From local resynchronization to global pattern recovery in the zebrafish segmentation clock** *eLife* **10**:e61358 https://doi.org/10.7554/eLife.61358

Uriu K, Morelli LG 2014) **Collective cell movement promotes synchronization of coupled genetic oscilla-tors** *Biophysical journal* **107**:514–526 https://doi.org/10.1016/j.bpj.2014.06.011

Uriu K, Morishita Y, Iwasa Y. 2010) **Random cell movement promotes synchronization of the segmen-tation clock** *Proceedings of the National Academy of Sciences* **107**:4979–4984 https://doi.org/10.1073/pnas.0907122107

Venzin OF, Oates AC 2020) **What are you synching about? Emerging complexity of Notch signaling in the segmentation clock** *Developmental biology* **460**:40–54 https://doi.org/10.1016/j.ydbio.2019.06.024

Wagner G, Pavlicev M, Cheverud J. 2007) **The road to modularity** *Nature Reviews Genetics* **8** https://doi.org/10.1038/nrg2267

Wagner GP, Altenberg L. 1996) **Perspective: Complex adaptations and the evolution of evolvability** *Evolution* **50** https://doi.org/10.1111/j.1558-5646.1996.tb02339.x

Webb AB, Lengyel IM, Jörg DJ, Valentin G, Jülicher F, Morelli LG, Oates AC 2016) **Persistence, period and precision of autonomous cellular oscillators from the zebrafish segmentation clock** *eLife* **5**:e08438 https://doi.org/10.7554/eLife.08438

Xiong F, Ma W, Bénazéraf B, Mahadevan L, Pourquié O 2020) **Mechanical coupling coordinates the co-elongation of axial and paraxial tissues in avian embryos** *Developmental Cell* **55**:354–366 https://doi.org/10.1016/j.devcel.2020.08.007

Author information

James E Hammond
Biology Department, University of Oxford, Oxford, United Kingdom
ORCID iD: 0000-0001-9603-3410

Ruth E Baker
Mathematical Institute, University of Oxford, Oxford, United Kingdom
ORCID iD: 0000-0002-6304-9333

Berta Verd
Biology Department, University of Oxford, Oxford, United Kingdom
ORCID iD: 0000-0001-9835-009X

For correspondence: berta.verdfernandez@biology.ox.ac.uk

Editors

Reviewing Editor
Claude Desplan
New York University, New York, United States of America

Senior Editor
Claude Desplan
New York University, New York, United States of America

Reviewer #1 (Public review):

Summary:

In this manuscript, Hammond et al. study robustness of the vertebrate segmentation clock against morphogenetic processes such as cell ingression, cell movement and cell division to ask whether the segmentation clock and morphogenesis are modular or not. The modularity of these two would be important for evolvability of the segmenting system. The authors adopt a previously proposed 3D model of the presomitic mesoderm (Uriu et al. 2021 eLife) and include new elements; different types of cell ingression, tissue compaction and cell cycles. Based on the results of numerical simulations that synchrony of the segmentation clock is robust, the authors conclude that there is a modularity in the segmentation clock and morphogenetic processes.

The presented results support the conclusion. The manuscript is clearly written.

Major comments from the original round of review:

[Optional] In both the current model and Uriu et al. 2021, coupling delay in phase oscillator model is not considered. Given that several previous studies (e.g. Lewis 2003, Herrgen et al. 2010, Yoshioka-Kobayashi et al. 2020) suggested the presence of coupling delays in Delta-Notch signaling, could the authors analyze the effect of coupling delay on robustness of the segmentation clock against morphogenetic processes?

Significance:

Synchronization of the segmentation clock has been studied by mathematical modeling, but most previous studies considered cells in a static tissue without morphogenesis. In the previous study by Uriu et al. 2021, morphogenetic processes such as cell advection due to tissue elongation, tissue shortening, and cell mobility were considered in synchronization. The current manuscript provides methodological advances in this aspect by newly including cell ingression, tissue compaction and cell cycle. In addition, the authors bring a concept of modularity and evolvability to the field of the vertebrate segmentation clock, which is new. On the other hand, the manuscript confirms that the synchronization of the segmentation clock is robust by careful simulations, but it does not propose or reveal new mechanisms for making it robust or modular. The main targets of the manuscript will be researchers working on somitogenesis and evolutionary biologists who are interested in evolution of developmental systems. The manuscript will also be interested by broader audiences, like developmental biologists, biophysicists, and physicists and computer scientists who are working on dynamical systems.

https://doi.org/10.7554/eLife.106316.1.sa3

Reviewer #2 (Public review):

Summary:

The manuscript from Hammond et al., investigates the modularity of the segmentation clock and morphogenesis in early vertebrate development, focusing on how these processes might independently evolve to influence the diversity of segment numbers across vertebrates.

Methodology: The study uses a previously published computational model, parameterized for zebrafish, to simulate and analyse the interactions between the segmentation clock and the morphogenesis of the pre-somitic mesoderm (PSM). Their model integrates cell advection, motility, compaction, cell division, and the synchronization of the embryo clock. Three

alternative scenarios of PSM morphogenesis were modeled to examine how these changes affect the segmentation clock.

Model System: The computational model system combines a representation of cell movements and the phase oscillator dynamics of the segmentation clock within a three-dimensional horseshoe-shaped domain mimicking the geometry of the vertebrate embryo PSM. The parameters used for the mathematical model are mostly estimated from previously published experimental findings.

Key Findings and Conclusions: (1) The segmentation clock was found to be broadly robust against variations in morphogenetic processes such as cell ingression and motility; (2) Changes in the length of the PSM and the strength of phase coupling within the clock significantly influenced the system's robustness; (3) The authors conclude that the segmentation clock and PSM morphogenesis exhibited developmental modularity (i.e. relative independence), allowing these two phenomena to evolve independently, and therefore possibly contributing to the diverse segment numbers observed in vertebrates.

Major comments from the original round of review:

(1) The key conclusion drawn by the authors (that there is robustness, and therefore modularity, between the morphogenetic cellular processes modeled and the embryo clock synchronization) stems directly from the modeling results appropriately presented and discussed in the manuscript.

The model comprises some strong assumptions, however all have been clearly explained and the parameterization choices are supported by experimental findings, providing biological meaning to the model. Estimated parameters are well explained, and seem reasonable assumptions (from the embryology perspective).

(2) This study, as is, achieves its proposed goal of evaluating the potential robustness of the embryo clock to changes in (some) morphogenetic processes. The authors do not claim that the model used is complete, and they properly identify some limitations, including the lack of cell-cell interactions. Given the recognized importance of cellular physical interactions for successful embryo development, including them in the model would be a significant addition in future studies.

(3) The authors have deposited all the code used for analysis in a public GitHub repository that is updated and available for the research community.

(4) In page 6, the authors justify their choice of clock parameters for cells ingressing the PSM: "As ingressing cells do not appear to express segmentation clock genes (Mara et al. (2007)), the position at which cells ingress into the PSM can create challenges for clock patterning, as only in the 'off' phase of the clock will ingressing cells be in-phase with their neighbors."

However, there are several lines of evidence (in chick and mouse), that some oscillatory clock genes are already being expressed as early as in the gastrulation phase (so prior to PSM ingression) (Feitas et al, 2001 [10.1242/dev.128.24.5139]; Jouve et al, 2002 [10.1242/dev.129.5.1107]; Maia-Fernandes at al, 2024 [10.1371/journal.pone.0297853]).

Question: Is this also true in zebrafish? (I.e. is there any recent experimental evidence that the clock genes are not expressed at ingression, since the paper cited to support this assumption is from 2007).

If they are expressed in zebrafish (as they are in mouse and chick), then the cell addition should have random clock gene periods when they enter the PSM and not start all with a constant initial phase of zero. Probably this will not impact the results since the cells will also

be out of phase with their neighbors when they "ingress", however, it will model more closely the biological scenario (and avoid such criticism).

Significance:

GENERAL ASSESSMENT

This study uses a previously published model to simulate alternative scenarios of morphogenetic parameters to infer the potential independence (termed here modularity) between the segmentation clock and a set of morphogenetic processes, arguing that such modularity could allow the evolution of more flexible body plans, therefore partially explaining the variability in the number of segments observed in the vertebrates. This question is fundamental and relevant, yet still poorly researched. This work provides a comprehensive simulation with a model that tries to simplify the many morphogenetic processes described in the literature, reducing it to a few core fundamental processes that allow drawing the conclusions sought. It provides theoretical insight to support a conceptual advance in the field of evolutionary vertebrate embryology.

ADVANCE

This study builds on a model recently published by Uriu et al. (eLife, 2021) that incorporates quantitative experimental data within a modeling framework including cell and tissue-level parameters, allowing the study of multiscale phenomena active during zebrafish embryo segmentation. Uriu's publication reports many relevant and often non-intuitive insights uncovered by the model, most notably the description of phase vortices formed by the synchronizing genetic oscillators interfering with the traveling-wave front pattern.

However, this model can be further explored to ask additional questions beyond those described in the original paper. A good example is the present study, which uses this mathematical framework to investigate the potential independence between two of the modeled processes, thereby extracting extra knowledge from it. Accordingly, the present study represents a step forward in the direction of using relevant theoretical frameworks to quantitatively explore the landscape of complex molecular hypotheses in silico, and with it shed some light on fundamental open questions or inform the design of future experiments in the lab.

The study incorporates a wide range of existing literature on the developmental biology of vertebrates. It comprehensively cites prior work, such as the foundational studies by Cooke and Zeeman on the segmentation clock and the role of FGF signaling in PSM development as discussed by Gomez et al. The literature properly covers the breadth of knowledge in this field.

AUDIENCE

Target audience: This study is relevant for fundamental research in developmental biology, specifically targeting researchers who focus on early embryo development and morphogenesis from both experimental and theoretical perspectives. It is also relevant for evolutionary biologists investigating the genetic factors that influence vertebrate evolution, as well as to computational biologists and bioinformatics researchers studying developmental processes and embryology.

Developmental researchers studying the segmentation clock in other vertebrate model organisms (namely mouse and chick), will find this publication especially valuable since it provides insights that can help them formulate new hypotheses to elucidate the molecular mechanisms of the clock (for example finding a set of evolutionarily divergent genes that might interfere with PSM length).
Additionally, this study provides a set of cellular parameters that have yet to be measured in

mouse and chick, therefore guiding the design of future experiments to measure them, allowing the simulation of the same model with sets of parameters from different vertebrate model organisms, therefore testing the robustness of the findings reported for zebrafish.

https://doi.org/10.7554/eLife.106316.1.sa2

Reviewer #3 (Public review):

Summary:

In this manuscript, Verd and colleagues explored how various biologically relevant factors influence the robustness of clock dynamics synchronization among neighboring cells within the context of somatogenesis, adapting a mathematical model presented by Urio et. al in 2021 in a similar context. Specifically they show that clock dynamics is robust to different biological mechanisms such as cell infusion, cellular motility, compaction-extension and cell-division. On the other hand , the length of Presomitic Mesoderm (PSM) and density of cells in it has a significant role in the robustness of clock dynamics. While the manuscript is well-written and provides clear descriptions of methods and technical details, it tends to be somewhat lengthy.

Major comments from original round of review:

(1) The authors mention that "...the model is three dimensional and so can quantitatively recapture the rates of cell mixing that we observe in the PSM". I am not convinced with this justification of using a 3D model. None of the effects the authors explore in this manuscript requires a three dimensional model or full physical description of the cellular mechanics such as excluded volume interaction etc. A one-dimensional model characterized by cell position along the arclength of PSM and somatic region and segmentation clock phase θ can incorporate all the physics authors described in this manuscript as well as significantly computationally cheap allowing the authors to explore the effect of different parameters in greater detail.

(2) I am not sure about the justification for limiting the quantification of phase synchrony in a very limited (one cell diameter wide) region at one end of the somatic part (Page 33 below Fig. 9). From my understanding of the manuscript, the segments appear in significant length anterior to this region. Wouldn't an ensemble average of multiple such one cell diameter wide regions in the somatic region be a more accurate metric for quantifying synchrony?

(3) While studying the effect of cellular ingression, the authors study three discrete modes-random, DP and DP+LV and show that in the DP+LV mode the clock synchrony becomes affected. I would like the authors to explore this in a continuous fashion from a pure DP ingression to Pure LV ingression and intermediates.

(4) While studying the effect of length and density of cells in PSM on cellular synchrony, the authors restrict to 3 values of density and 6 values of PSM length keeping the other parameter constant. I would be interested to see a phase diagram similar to Fig. 7 in the two dimensional parameter space of L and ρ0. I am curious if a scaling relation exists for the parameter values that partition the parameter space with and without synchrony.

(5) Both in the abstract and introduction, the authors discuss at a great length about the variability in the number of segments. I am curious how the number and width of the segments observed depend on different parameters related to cellular mechanics and the segmentation clock ?

(6) The authors assume that the phase dynamics of the chemical network may be described by an oscillator with constant frequency. For the completeness of the manuscript, the author

should discuss in detail, for which chemical networks this is a good assumption.

(7) Figure 3 and the associated text shows no effect of the cellular motility profile in the synchrony of the segmentation clock. This may be moved to the supplementary considering the length of this manuscript.

Significance:

The manuscript answers some important questions in the synchrony of segmentation clock in the vertebrates utilizing a model published earlier. However, the presented result is incomplete in some aspects (points 2 to 5 of section A) and that could be overcome by a more detailed analysis using a simpler one dimensional (point 1 of section A). I believe this manuscript could be of interest to an intersecting audience of developmental biologists, systems biologists, and physicists/engineers interested in dynamical systems.

[Editors' note: the authors have responded comprehensively to the reviews from Review Commons.]

https://doi.org/10.7554/eLife.106316.1.sa1

Author response:

> ***Reviewer #1 (Evidence, reproducibility and clarity):***
>
> *Summary:*
>
> *In this manuscript, Hammond et al. study robustness of the vertebrate segmentation clock against morphogenetic processes such as cell ingression, cell movement and cell division to ask whether the segmentation clock and morphogenesis are modular or not. The modularity of these two would be important for evolvability of the segmenting system. The authors adopt a previously proposed 3D model of the presomitic mesoderm (Uriu et al. 2021 eLife) and include new elements; different types of cell ingression, tissue compaction and cell cycles. Based on the results of numerical simulations that synchrony of the segmentation clock is robust, the authors conclude that there is a modularity in the segmentation clock and morphogenetic processes. The presented results support the conclusion. The manuscript is clearly written. I have several comments that could help the authors further strengthen their arguments.*
>
> *Major comment:*
>
> *[Optional] In both the current model and Uriu et al. 2021, coupling delay in phase oscillator model is not considered. Given that several previous studies (e.g. Lewis 2003, Herrgen et al. 2010, Yoshioka-Kobayashi et al. 2020) suggested the presence of coupling delays in DeltaNotch signaling, could the authors analyze the effect of coupling delay on robustness of the segmentation clock against morphogenetic processes?*

We thank the reviewer for the suggestion. Owing to the computational demands of including such a delay in the model, we cannot feasibly repeat every simulation analysed here in the presence of delay, and would like to note that the increased computational demand that delays put on the simulations is also the reason why Uriu et al 2021 did not include it, as stated in their published exchange with reviewers. However, analogous to our analysis in figure 7, we can analyse how varying the position of progenitor cell ingression affects synchrony in the presence of the coupling delay measured in zebrafish by Herrgen et al. (2010). We show this analysis in a new figure 8 (8B, specifically), on page 21, and discuss its implications in the text on pages 2022. Our analysis reveals that the model cannot recover synchrony using the default parameters used by Uriu et al. (2021) and reveal a much stronger

dependence on the rate of cell mixing (vs) than shown in the instantaneous coupling case (cf. figure 7). However, by systematically varying the value of the delay we find that a relatively minor increase in the delay is sufficient to recover synchrony using the parameter set of Uriu et al. (see figure 8C). Repeating this across the three scenarios of cell ingression we see that the combination of coupling strength and delay determine the robustness of synchrony to varying position of cell ingression. This suggests that the combination of these two parameters constrain the evolution of morphogenesis.

> *Minor comments:*
>
> *- PSM radius and oscillation synchrony are both denoted by the same alphabet r. The authors should use different alphabets for these two to avoid confusion.*

We thank the reviewer for spotting this. This has now been changed throughout to rT, as shorthand for ‘radius of tissue’.

> *- page 5 Figure 1 caption: (x-x_a/L) should be (x-x_a)/L.*

We thank the reviewer for spotting this. This has now been corrected.

> *- Figure 3C: Description of black crosses in the panels is required in the figure legend.*

Thank you for spotting this. The legend has now been corrected.

> *- Figure 3C another comment: In this panel, synchrony r at the anterior PSM is shown. It is true that synchrony at anterior PSM is most relevant for normal segment formation. However, in this case, the mobility profile is changed, so it may be appropriate to show how synchrony at mid and posterior PSM would depend on changes in mobility profile. Is synchrony improved by cell mobility at the region where cell ingression happens?*

We thank the reviewer for the suggestion. We have now plotted the synchrony along the AP axis for varying motility profiles, and this can be seen in figure 3 supplement 1, and is briefly discussed in the text on page 11. We show that while the synchrony varies with x-position (as already expected, see figure 2), there is no trend associated with the shape of the motility profile.

> *- In page 12, the authors state that "the results for the DP and DP+LV cases are exactly equal for L = 185 um, as …. and the two ingression methods are numerically equivalent in the model". I understood that in this case two ingression methods are equivalent, but I do not understand why the results are "exactly" equal, given the presence of stochasticity in the model.*

These results can be exactly equal despite the simulations being stochastic because they were both initialised using the same ‘seed’ in the source code. However, we now see that this might be confusing to the reader, and we have re-generated this figure but this time initialising the simulations for each ingression scenario using a different seed value. This is now reflected in the text on page 12 and in figure 4.

> *- The authors analyze the effect of cell density on oscillation synchrony in Fig. 4 and they mention that higher density increases robustness of the clock by increasing the average number of interacting neighbours. I think it would be helpful to plot the average number of neighbouring cells in simulations as a function of density to quantitatively support the claim.*

We thank the reviewer for their suggestion. Distributions of neighbour numbers for exemplar simulations with varying density can now be found in figure 4 supplementary figure 1 and are referred to in the text on page 11.

> *- The authors analyze the effect of PSM length on synchrony in Fig. 4. I think kymographs of synchrony r as shown in Fig. 2D would also be helpful to show that indeed cells get synchronized while advecting through a longer PSM.*

We thank the reviewer for their suggestion and agree that visualising the data in this way is an excellent idea. We have generated the suggested kymographs and added them to figure 4 as supplements 2 and 4, and discussed these results in the text on page 12.

> *- I understand that cells in M phase can interact with neighboring cells with the same coupling strength kappa in the model, although their clocks are arrested. If so, this aspect should be also mentioned in the main text in page 16, as this coupling can be another noise source for synchrony.*

We agree this is an important clarification. We explicitly state this, and briefly justify our choice, in the text on page 16.

> *- Figure 5-figure supplement 2: panel labels A, B, C are missing.*

Thank you for bringing this to our attention. These have now been added.

> *– Figure 5-figure supplement 3: panel labels A, B, C are missing.*

Thank you for bringing this to our attention. These have now been added.

> ***Reviewer #1 (Significance):***
>
> *Synchronization of the segmentation clock has been studied by mathematical modeling, but most previous studies considered cells in a static tissue without morphogenesis. In the previous study by Uriu et al. 2021, morphogenetic processes such as cell advection due to tissue elongation, tissue shortening, and cell mobility were considered in synchronization. The current manuscript provides methodological advances in this aspect by newly including cell ingression, tissue compaction and cell cycle. In addition, the authors bring a concept of modularity and evolvability to the field of the vertebrate segmentation clock, which is new. On the other hand, the manuscript confirms that the synchronization of the segmentation clock is robust by careful simulations, but it does not propose or reveal new mechanisms for making it robust or modular. The main targets of the manuscript will be researchers working on somitogenesis and evolutionary biologists who are interested in evolution of developmental systems. The manuscript will also be interested by broader audiences, like developmental biologists, biophysicists, and physicists and computer scientists who are working on dynamical systems.*

We thank the reviewer for their interest in our manuscript and for acknowledging us as one of the first to address the modularity and evolvability of somitogenesis. We hope that this work will encourage others to think about these concepts in this system too.

In the original submission, we identified a high enough coupling strength as the main mechanism underlying the identified modularity in somitogenesis. Since, we have included an analysis of the coupling delay and find that it is the interplay between coupling strength and coupling delay that mediate the identified modularity, allowing PSM morphogenesis and the segmentation clock to evolve independently in regions of parameter space that are

constrained and determined by the interplay between these two parameters. We have now added an extra figure (figure 8) where we explore this interplay and have discussed it at length in the last section of the results and in the discussion. We again thank the reviewer for encouraging us to include delays in our analysis.

> ***Reviewer #2 (Evidence, reproducibility and clarity):***
>
> *SUMMARY*
>
> *The manuscript from Hammond et al., investigates the modularity of the segmentation clock and morphogenesis in early vertebrate development, focusing on how these processes might independently evolve to influence the diversity of segment numbers across vertebrates.*
>
> *Methodology: The study uses a previously published computational model, parameterized for zebrafish, to simulate and analyse the interactions between the segmentation clock and the morphogenesis of the pre-somitic mesoderm (PSM). Their model integrates cell advection, motility, compaction, cell division, and the synchronization of the embryo clock. Three alternative scenarios of PSM morphogenesis were modeled to examine how these changes affect the segmentation clock.*
>
> *Model System: The computational model system combines a representation of cell movements and the phase oscillator dynamics of the segmentation clock within a three-dimensional horseshoe-shaped domain mimicking the geometry of the vertebrate embryo PSM. The parameters used for the mathematical model are mostly estimated from previously published experimental findings.*
>
> *Key Findings and Conclusions: (1) The segmentation clock was found to be broadly robust against variations in morphogenetic processes such as cell ingression and motility; (2) Changes in the length of the PSM and the strength of phase coupling within the clock significantly influenced the system's robustness; (3) The authors conclude that the segmentation clock and PSM morphogenesis exhibited developmental modularity (i.e. relative independence), allowing these two phenomena to evolve independently, and therefore possibly contributing to the diverse segment numbers observed in vertebrates.*
>
> *MAJOR COMMENTS*
>
> *(1) The key conclusion drawn by the authors (that there is robustness, and therefore modularity, between the morphogenetic cellular processes modeled and the embryo clock synchronization) stems directly from the modeling results appropriately presented and discussed in the manuscript. The model comprises some strong assumptions, however all have been clearly explained and the parameterization choices are supported by experimental findings, providing biological meaning to the model. Estimated parameters are well explained and seem reasonable assumptions (from the embryology perspective).*

We thank the reviewer for their positive comments about our work

> *(2) This study, as is, achieves its proposed goal of evaluating the potential robustness of the embryo clock to changes in (some) morphogenetic processes. The authors do not claim that the model used is complete, and they properly identify some limitations, including the lack of cellcell interactions. Given the recognized importance of cellular physical interactions for successful embryo development, including them in the model would be a significant addition in future studies.*

We would like to clarify that the model does include cell-cell interactions as cells interact with their neighbours' clock phase to synchronise and to avoid occupying the same physical space.

> *(3) The authors have deposited all the code used for analysis in a public GitHub repository that is updated and available for the research community.*

We support open source coding practices.

> *(4) In page 6, the authors justify their choice of clock parameters for cells ingressing the PSM: "As ingressing cells do not appear to express segmentation clock genes (Mara et al. (2007)), the position at which cells ingress into the PSM can create challenges for clock patterning, as only in the 'off' phase of the clock will ingressing cells be in-phase with their neighbours." However, there are several lines of evidence (in chick and mouse), that some oscillatory clock genes are already being expressed as early as in the gastrulation phase (so prior to PSM ingression) (Feitas et al, 2001 [10.1242/dev.128.24.5139]; Jouve et al, 2002 [10.1242/dev.129.5.1107]; Maia-Fernandes at al, 2024 [10.1371/journal.pone.0297853]) Question: Is this also true in zebrafish? (I.e. is there any recent experimental evidence that the clock genes are not expressed at ingression, since the paper cited to support this assumption is from 2007). If they are expressed in zebrafish (as they are in mouse and chick), then the cell addition should have random clock gene periods when they enter the PSM and not start all with a constant initial phase of zero. Probably this will not impact the results since the cells will also be out of phase with their neighbours when they "ingress", however, it will model more closely the biological scenario (and avoid such criticism).*

We thank the reviewer for their comments. While it is known that in zebrafish the clock begins oscillating during epiboly and before the onset of segmentation (Riedel-Kruse et al., 2007), to our knowledge no-one has examined whether posteriorly or laterally ingressing progenitor cells express clock genes prior to their ingression into the PSM, which occurs later in development than the first oscillations which give rise to the first somites. We have not found any published evidence of her/hes gene expression in the dorsal donor tissues or lateral tissues surrounding the PSM, however we acknowledge that this has not been actively studied before and our assumption relies on an absence of evidence, rather than evidence of absence.

However, we agree with the reviewer that one should include such an analysis for completeness, and we have now generated additional simulations where progenitor cells ingress with a random clock phase. This data is presented in figure 2 supplement 1 and mentioned in the main text on page 9.

> *MINOR COMMENTS*
>
> *(1) The citations are appropriate and cover the major labs that have published work related to this study (although with some overrepresentation of the lab that published the model used).*

We have cited the vast literature on somitogenesis to the best of our ability and do recognise that the work of the Oates lab appears prominently, but this is probably because their experimental data were originally used to parametrise the model in Uriu et al. 2021.

> *(2) The text is clear, carefully written, and both the methods and the reasoning behind them are clearly explained and supported by proper citations.*

We are very glad to see that the reviewer found that the manuscript was clearly presented.

> *(3) The figures are comprehensive, properly annotated, with explanatory self-contained legends. I have no comments regarding the presentation of the results.*

Thank you

> *(4) Minor suggestions:*
>
> *a. Page 26: In the Cell addition sub-section of the Methods section, correct all instances where the word domain is used, but subdomain should be used (for clarity and coherence with the description of the model, stated as having a single domain comprising 3 subdomains).*

We thank the reviewer for raising this, this is a good point. We have now corrected to 'subdomain' where appropriate.

> *b. Page 32: Table 1. Parameter values used in our work, unless otherwise stated -> Suggestion: Add a column with the individual citations used for each parameter (to facilitate the confirmation of each corresponding reference).*

Thank you for the suggstion, we have now done this (see table 1 page 36).

> ***Reviewer #2 (Significance):***
>
> *GENERAL ASSESSMENT*
>
> *This study uses a previously published model to simulate alternative scenarios of morphogenetic parameters to infer the potential independence (termed here modularity) between the segmentation clock and a set of morphogenetic processes, arguing that such modularity could allow the evolution of more flexible body plans, therefore partially explaining the variability in the number of segments observed in the vertebrates. This question is fundamental and relevant, yet still poorly researched. This work provides a comprehensive simulation with a model that tries to simplify the many morphogenetic processes described in the literature, reducing it to a few core fundamental processes that allow drawing the conclusions seeked. It provides theoretical insight to support a conceptual advance in the field of evolutionary vertebrate embryology.*
>
> *ADVANCE*
>
> *This study builds on a model recently published by Uriu et al. (eLife, 2021) that incorporates quantitative experimental data within a modeling framework including cell and tissue-level parameters, allowing the study of multiscale phenomena active during zebrafish embryo segmentation. Uriu's publication reports many relevant and often non-intuitive insights uncovered by the model, most notably the description of phase vortices formed by the synchronizing genetic oscillators interfering with the traveling-wave front pattern. However, this model can be further explored to ask additional questions beyond those described in the original paper. A good example is the present study, which uses this mathematical framework to investigate the potential independence between two of the modeled processes, thereby extracting extra knowledge from it. Accordingly, the present study represents a step forward in the direction of using relevant theoretical frameworks to quantitatively explore the landscape of complex molecular hypotheses in silico, and with it shed some light on fundamental open questions or inform the design of future experiments in the lab.*
>
> *The study incorporates a wide range of existing literature on the developmental biology of vertebrates. It comprehensively cites prior work, such as the foundational studies by*

Cooke and Zeeman on the segmentation clock and the role of FGF signaling in PSM development as discussed by Gomez et al. The literature properly covers the breadth of knowledge in this field.

AUDIENCE

Target audience | This study is relevant for fundamental research in developmental biology, specifically targeting researchers who focus on early embryo development and morphogenesis from both experimental and theoretical perspectives. It is also relevant for evolutionary biologists investigating the genetic factors that influence vertebrate evolution, as well as to computational biologists and bioinformatics researchers studying developmental processes and embryology.

Developmental researchers studying the segmentation clock in other vertebrate model organisms (namely mouse and chick), will find this publication especially valuable since it provides insights that can help them formulate new hypotheses to elucidate the molecular mechanisms of the clock (for example finding a set of evolutionarily divergent genes that might interfere with PSM length). Additionally, this study provides a set of cellular parameters that have yet to be measured in mouse and chick, therefore guiding the design of future experiments to measure them, allowing the simulation of the same model with sets of parameters from different vertebrate model organisms, therefore testing the robustness of the findings reported for zebrafish.

Reviewer #3 (Evidence, reproducibility and clarity):

In this manuscript, Verd and colleagues explored how various biologically relevant factors influence the robustness of clock dynamics synchronization among neighboring cells within the context of somatogenesis, adapting a mathematical model presented by Urio et. al in 2021 in a similar context. Specifically they show that clock dynamics is robust to different biological mechanisms such as cell infusion, cellular motility, compaction-extension and cell-division. On the other hand , the length of Presomitic Mesoderm (PSM) and density of cells in it has a significant role in the robustness of clock dynamics. While the manuscript is well-written and provides clear descriptions of methods and technical details, it tends to be somewhat lengthy.

Below are the comments I would like the authors to address:

(1) The authors mention that "...the model is three dimensional and so can quantitatively recapture the rates of cell mixing that we observe in the PSM". I am not convinced with this justification of using a 3D model. None of the effects the authors explore in this manuscript requires a three dimensional model or full physical description of the cellular mechanics such as excluded volume interaction etc. A one-dimensional model characterized by cell position along the arclength of PSM and somatic region and segmentation clock phase θ can incorporate all the physics authors described in this manuscript as well as significantly computationally cheap allowing the authors to explore the effect of different parameters in greater detail.

One of the main objectives of the work we present in this manuscript is to assess how the evolution of PSM morphogenesis affects, or does not affect, segment patterning. The PSM is a three-dimensional tissue with differing cell rearrangement dynamics along its anterior-posterior axis. In addition, PSM dimension, density, the rearrangement rate, and patterns of cell ingression all vary across vertebrate species, and they are functional, especially cell mixing as it promotes synchronisation and drives elongation. In order to answer questions on the modularity of somitogenesis we therefore consider it absolutely necessary to include a three-dimensional representation of the PSM that captures single cells and their movements.

In addition, this will allow us, as Reviewer #2 also pointed out, to reparametrize our model using species-specific data as it becomes available.

While the reviewer is right in that lower dimensional representations would be computationally more efficient, and are generally more tractable, it would not be possible to represent cell mixing in one dimension, as this happens in three dimensions. One could perhaps encode the synchrony-promoting effect of cell mixing via some coupling function $\kappa(x)$ that increases towards the posterior, however it is unclear what existing biological data one could use to parameterise this function or determine its form. Cell mixing can be modelled in a two-dimensional framework, however this cannot quantitatively recapture the rate of cell mixing observed *in vivo*, which is an advantage of this model.

Furthermore, it is unclear how one would simulate processes such as compactionextension using a one-dimensional model. The two different scenarios of cell ingression which we consider can also not be replicated in a one-dimensional model, as having a population of cells re-acquiring synchrony on the dorsal surface of the tissue while new material is added to the ventral side, creating asynchrony, is qualitatively different than a one-dimensional scenario where cells are introduced continuously along the spatial axis.

> *(2) I am not sure about the justification for limiting the quantification of phase synchrony in a very limited (one cell diameter wide) region at one end of the somatic part (Page 33 below Fig. 9). From my understanding of the manuscript, the segments appear in significant length anterior to this region. Wouldn't an ensemble average of multiple such one cell diameter wide regions in the somatic region be a more accurate metric for quantifying synchrony?*

Indeed, such a metric (e.g. as that used by Uriu et al. to quantify synchrony along the xaxis) would be more accurate for determining synchrony within the PSM. However, as per the clock and wavefront model of somitogenesis, only synchrony at the very anterior of the PSM (or at the wavefront, equivalently) is functional for somitogenesis and thus evolution. Therefore, we restrict our analysis to the anterior-most region of the PSM. We now further justify this in the main text on page 9.

> *(3) While studying the effect of cellular ingression, the authors study three discrete modes- random, DP and DP+LV and show that in the DP+LV mode the clock synchrony becomes affected. I would like the authors to explore this in a continuous fashion from a pure DP ingression to Pure LV ingression and intermediates.*

We thank the reviewer for this suggestion; this is a very interesting question. We are currently working on a related computational and experimental project to address the question of how PSM morphogenesis can change over evolutionary time to evolve the different modes that we see across species. As part of this work, we are running precisely the simulations suggested by the reviewer to find regions of parameter space in which all the relevant morphogenetic processes can freely evolve. While interesting, this work is however outside the scope of the current manuscript.

> *(4) While studying the effect of length and density of cells in PSM on cellular synchrony, the authors restrict to 3 values of density and 6 values of PSM length keeping the other parameter constant. I would be interested to see a phase diagram similar to Fig. 7 in the two-dimensional parameter space of L and ρ0. I am curious if a scaling relation exists for the parameter values that partition the parameter space with and without synchrony.*

We thank the reviewer for their suggestion and agree that this would constitute an interesting addition to the manuscript. We have now generated these data, which are shown

in figure 4 supplement 5 and mentioned on page 13. We see no clear relationship between these two variables when co-varying in the presence of random ingression.

> *(5) Both in the abstract and introduction, the authors discuss at a great length about the variability in the number of segments. I am curious how the number and width of the segments observed depend on different parameters related to cellular mechanics and the segmentation clock ?*

We thank the reviewer for this question. It was not clear to us if this was something the reviewer wants us to address in the study's background and introduction, or an analysis we should include in the results. Therefore, we have responded to both comprehensively below:

The prevailing conceptual framework for understanding this is the clock and wavefront model (Cooke and Zeeman, 1976), which posits that the somite length is inversely proportional to the frequency of the clock relative to the speed of the wavefront, and that the total number of segments is the relative frequency multiplied by the total duration of somitogenesis.

Experimentally we know that the frequency is determined in part by the coupling strength (Liao, Jorg, and Oates, 2016), and from comparative embryological studies (Gomez et al., 2008; Steventon et al., 2016) we know that changes in the elongation dynamics of the PSM correlate with changes in somite number, presumably by altering the total duration of somitogenesis (Gomez et al., 2009). These changes in elongation are thought to be driven by the changes in cell and tissue mechanics we test in our manuscript.

Within our model, we cannot in general predict how the number of segments responds to changes in either clock parameters or cell mechanical parameters, as we lack understanding of what causes somitogenesis to cease; this is thus not encoded in our model and segmentation can in principle proceed indefinitely. Therefore, we have not performed this analysis.

Similarly, we have not included an analysis of somite length. This is for two reasons: 1) as per the clock and wavefront model, the frequency at the PSM anterior (which we analyse) is equivalent to this measurement, as we assume (in general) the wavefront ($x = x_{a}$) is inertial. 2) the length of the nascent somite is not thought to be of much relevance to the adult phenotype, and by extension evolution. Somites undergo cell division and growth soon after their patterning by the segmentation clock, therefore their final size does not majorly depend on the dynamics of the segmentation clock. Rather, the main function of the clock is to control their number (and polarity).

> *(6) The authors assume that the phase dynamics of the chemical network may be described by an oscillator with constant frequency. For the completeness of the manuscript, the author should discuss in detail, for which chemical networks this is a good assumption.*

We thank the reviewer for their suggestion and now justify this assumption in the methods on page 31.

Such an assumption is appropriate for the segmentation clock, as the clock in the posterior of the PSM is thought to oscillate with a constant frequency, at least for the majority of somitogenesis although the frequency of somite formation slows towards the end of this process in zebrafish (Giudicelli et al., 2007, PLoS Biol.). In addition, PSM cells isolated and cultured in the presence of FGF (thus replicating the signalling environment of the posterior PSM) will continue to exhibit her1 oscillations with an apparently constant frequency (Webb et al., 2016).

We note that such formulations are widely used within the segmentation clock literature (e.g. Riedel-Kruse et al., 2007, Morelli et al., 2009).

> *(7) Figure 3 and the associated text shows no effect of the cellular motility profile in the synchrony of the segmentation clock. This may be moved to the supplementary considering the length of this manuscript.*

Thank you for the suggestion. However, we would argue that the lack of effect is a crucial result when discussing modularity. Reviewer #2 agrees with this assessment.

> ***Reviewer #3 (Significance):***
>
> *The manuscript answers some important questions in the synchrony of segmentation clock in the vertebrates utilizing a model published earlier. However, the presented result is incomplete in some aspects (points 2 to 5 of section A) and that could be overcome by a more detailed analysis using a simpler one dimensional (point 1 of section A). I believe this manuscript could be of interest to an intersecting audience of developmental biologists, systems biologists, and physicists/engineers interested in dynamical systems.*

https://doi.org/10.7554/eLife.106316.1.sa0